Two stochastic processes shape diverse senescence patterns in a single-cell organism

Short title: Stochastic processes shape senescence

Ulrich K. Steiner*[1,2,3,4], Adam Lenart[1‡], Ming Ni[3,4,5‡], Peipei Chen[3,6], Xiaohu Song[3], François Taddei[3,4], Ariel B. Lindner[3,4†], & James W. Vaupel[1†]

1

2   [1] Center on Population Dynamics, Campusvej 55, 5230 Odense, Denmark

3   [2] Biology Department, University of Southern Denmark, Campusvej 55, 5230 Odense, Denmark

4   [3] Center for Research and Interdisciplinarity, Paris Descartes University, 75014, Paris, France

5   [4] INSERM U1001, 75014 Paris, France

6   [5] Current address: BGI Shenzhen, Shenzhen, China

7   [6] Current address: National Center for Nanoscience and Technology, Beijing, China

8

9

10   ***Corresponding author: usteiner@biology.sdu.dk**

11   [†] Joint senior authors

12   [‡] Equal contribution of second authors

13   Keywords: senescence, mechanisms of aging, evolution of aging, asymmetry, damage accumulation,

14   aging models,

15   Authors contributions: UKS designed the study, UKS, MN & PC performed the experiments, UKS,

16   AL, XS analyzed the data, all authors substantially contributed to discussions and writing the

17   manuscript, UKS wrote the first and final draft of the manuscript.

18

Abstract

Despite advances in aging research, a multitude of aging models, and empirical evidence for diverse senescence patterns, understanding is lacking of the biological processes that shape senescence, both for simple and complex organisms. We show that for a isogenic *Escherichia coli* bacterial population senescence results from two stochastic processes. A primary random deterioration process within the cell, such as generated by random accumulation of damage, leads to an exponential increase in mortality early in life followed by a late age mortality plateau; a secondary process of stochastic asymmetric transmission of an unknown factor at cell fission influences mortality. This second process is required to explain the difference between the classical mortality plateaus detected for young mothers' offspring and the near non-senescence of old mothers' offspring as well as the lack of a mother offspring correlation in age at death. We observed that life span is predominantly determined by underlying stochastic stage dynamics. Our findings support models based on stage-specific actions of alleles for the evolution of senescence. This support might be surprising since these models that have not specifically been developed in the context of simple, single cell organisms. We call for exploration of similar stochastic influences beyond simple organisms.

Introduction

One of the major challenges for biodemographic research on aging is to understand what drives senescence patterns (Vaupel et al. 1998, López-Otín et al. 2013). This challenge is illustrated by the variety of aging models that assume different, as yet unverified generating processes (Hamilton 1966, Kirkwood 2005, Wachter et al. 2014). Prominent — mutually not exclusive — evolutionary theories of senescence, such as William's antagonistic pleiotropy hypothesis (Williams 1957), or Medawar's mutation accumulation hypothesis (Medawar 1952), provide general predictions about uniform

42   senescence patterns across many taxa (Hamilton 1966). However, these generalities have been

43   questioned both theoretically and empirically by illustrating how negligible and negative-senescence can

44   theoretically be achieved and been empirically found in various species (Vaupel et al. 2004, Jones et al.

45   2014). Despite an extensive literature on mechanistic approaches of aging, the generating processes that

46   drive such diversity in senescence patterns remain opaque (López-Otín et al. 2013). Mechanistic

47   approaches to aging identify a multitude of underlying biochemical, molecular and organismal

48   mechanisms that relate to the decline of function with age, many of which are rooted in direct or indirect

49   oxidative processes (Kirkwood 2005, López-Otín et al. 2013). Examples include age-related

50   mitochondrial dysfunction, telomere shortening, stem cell exhaustion, genotypic instability, epigenetic

51   alterations, accumulation of damaged proteins and general loss of proteostasis (Lindner and Demarez

52   2009, Tyedmers et al. 2010, López-Otín et al. 2013). Yet, researchers have not conclusively determined

53   whether such mechanisms are a cause or consequence of aging. This failure may be due to the complexity

54   of model systems of aging. As a consequence, it is difficult to relate these mechanisms directly to the

55   observed demographic patterns (Tyedmers et al. 2010, López-Otín et al. 2013, Denoth Lippuner et al.

56   2014). Only such linkage — between mechanisms and senescence patterns — can elucidate generating

57   processes that underlie the various theories and aspects of aging.

58

59   Aging in bacteria has been established over the last one and a half decades and thereby provided a

60   simple biological system to study aging (Ackermann et al. 2003, Stewart et al. 2005). Before, bacteria

61   have been thought to not age (Williams 1957), because they normally fission into two equal sized

62   progeny. These progeny were assumed to be identical, that is, the original mother cell would die when

63   fissioning and leaves two identical daughters (Johnson and Mangel 2006, Tyedmers et al. 2010). This

64   perspective has changed because the resulting progeny are phenotypically unequal (Tyedmers et al.

3

65   2010). This asymmetry among the progeny is manifested by asymmetry of intracellular content at cell

66   fission and between carrying old and newly formed cellular poles (Stewart et al. 2005, Lindner et al.

67   2008). Here, we follow the convention of old pole and new pole cells, being referred to as mother and

68   daughter cell respectively (Fig. 1), to track the age of individual cells (Stewart et al. 2005). It has been

69   shown that mother cells have a higher probability to accumulate misfolded protein and grow slower as

70   compared to their daughter cells, but a causal relationship to mortality was not established (Lindner et

71   al. 2008). From a theoretical point of view asymmetry is required to rejuvenate some cells in order to

72   prevent whole population aging. Otherwisepopulations would accumulate more and more damage if

73   perfect symmetric fissions occurred and damage accumulation accedes damage repair and dilution due

74   to growth and fission (Ackermann et al. 2007, Evans and Steinsaltz 2007).

75

76   Here, we reveal characteristics of the underlying aging processes by inference from observed senescence

77   patterns. We achieve this aim by quantifying demographic parameters of a simple biological system,

78   isogenic individual *E. coli* bacteria cells, under highly controlled environmental conditions. We used a

79   high-throughput microfluidic device (Fig. 1; movie S1) to track individual cells throughout their lives

80   (Wang et al. 2010, Gasset-Rosa et al. 2014, Jouvet et al. 2017). Two types of cells were tracked: early

81   daughter cells and late daughter cells (Fig.1). A late daughter cell is the last daughter cell produced by

82   an early daughter and hence an offspring of an old mother. An early daughter cell is the offspring of a

83   young mother since they were haphazardly extracted from a population that grew exponentially.

84   According to stable stage population theories such exponentially growing populations are vastly

85   dominated by young cells (Caswell 2001)(Fig. S1). We expect early daughters to hold little or no

86   deterioration or damage at birth, whereas late daughters are likely be born with some damage. In this

87   study, we use damage as a synonym for any unknown aging factor that leads to deterioration and

4

88   increased mortality. We use this synonym because many aging factors are assumed to be accumulated

89   damage caused by oxidative processes (Kirkwood et al. 2005, López-Otín et al. 2013). A third group of

90   cells, resembling the late daughter type are the last daughter cells produced by the late daughters, which

91   we call second generation late daughters (Results only in SI1). Our definition of mother and daughter

92   cells builds on the concept of cell polarity for both early daughter and late daughter cells to track the age

93   of cells and distinguish between the mothers (old pole cell) and the daughters (new pole cell) (Fig.1).

94

95   **Material and Methods**

96   For brevity we only provide in this section an overview of the methods. For more detailed methodological

97   information on strains and growth conditions, time-lapse imaging, image analysis, determining death and

98   estimating demographic parameters, statistical analyses, the simulations please see the supplemental

99   information.

100

101   We collected data in two independent sets of experiments. We loaded *E. coli* K12-derived MG1655 strain

102   cells into a designed microfluidic (PDMS) chip (Wang et al. 2010, Gasset-Rosa et al. 2014, Jouvet et al.

103   2017) from an exponentially growing culture in supplemented minimum media M9. During each

104   experiment, we acquired 77 hours of time lapse phase-contrast imaging (15 frames/hour for each of the

105   2x44 fields followed) using a temperature-controlled inverted microscope, at 43°C with an accuracy of

106   the temperature control at the chip of ±0.1°C (note within the chip temperature should be even more

107   closely controlled due to some buffering of the chip). We used 43°C to accelerate the aging process and

108   thereby shorten the time the system needed to run under stable conditions. Such stability was particularly

109   important to accurately track late daughter and second generation late daughter cells. Increasing

110   temperature up to 43 °C scales senescence patterns, but does not alter the shape of patterns (Jouvet &

111   Steiner unpublished). At 44 °C patterns got unstable and cells were not viable over longer time periods

112   (results not presented). The rod-shaped bacteria cells grew in dead end side channels of a microfluidic

113   chip, with the focal cells trapped at the end of the side channels, and we tracked them over their lifespan

114   (Fig. 1; movie S1). We used customized image analysis to generate the demographic data (lifespan, cell

115   elongation rate, cell size, and time of each division).

116

117   We assured by starting the experiments with exponentially growing cells that the initial loaded cells are

118   descendants of young mothers (i.e. they are early daughter cells) (Fig. S1). At the end of their lives, these

119   early daughter cells produced a last daughter (late daughters) that then became the next bottom-most cell

120   trapped at the end of the respective growth channel. Therefore, we could directly compare mother and

121   daughter cells. Note that the late daughters are not born at the same time (main text Fig. 2 E, F). The late

122   daughter cells produced another generation of late daughter cells at the end of their lives (second

123   generation late daughter cells) for which the results are shown in Fig. S2-8, Table S1-3. Analysis on the

124   empirical data were done in program R (R Core Team 2016) using general linear, generalized linear, and

125   non-linear models. Models were selected based on information criteria (AIC) (Burnham and Anderson

126   1998) or based on differential evolution algorithm for global optimization (R package DEoptim).

127

128   Simulations and extending random deterioration models.

129   For the extended random deterioration model, we first estimated parameters by fitting a fixed frailty

130   model — a Gamma-Gompertz-Makeham (GGM) model — to the observed survival data of the early

131   daughter cells (Yashin et al. 1994, Missov and Vaupel 2015). We then translated these fitted GGM model

132   parameters to an extended random deterioration process model, an extended LeBras type deterioration

133   model (Le Bras 1976). In doing so, we took advantage of mathematical similarities between the two

6

134   types of models, even though they are biologically distinct (Yashin et al. 1994, Missov and Vaupel 2015).

135   With these random deterioration model parameters we could estimate the probability matrix of an

136   individual being at stage i at age x. Microsimulations based on these models provided stage at death

137   distribution. For the late daughters, we assumed that they are born at a scaled version of the same damage

138   stage in which their mothers died. We also assumed that late daughters accumulate damage at the same

139   rates as early daughters do, i.e. same probabilities to transition to a higher damage state of early and late

140   daughters. We further assumed that the amount of accumulated damage in late daughters had the same

141   effect on mortality than on early daughters, that is, early and late daughter cells are not fundamentally

142   different except that late daughters are born in different damage stages, while early daughters start their

143   lives without damage, but the baseline mortality (Makeham term) can be interpreted as some starting

144   level of damage even for early daughters. Our model simplifies the biological system substantially in as

145   much as no repair of damage or purging of damage through asymmetric division at cell fission is

146   considered. Damage accumulates unidirectionally, mortality increases exponentially with accumulated

147   damage, and each cell suffers from an age-independent baseline mortality risk (Makeham term).

148

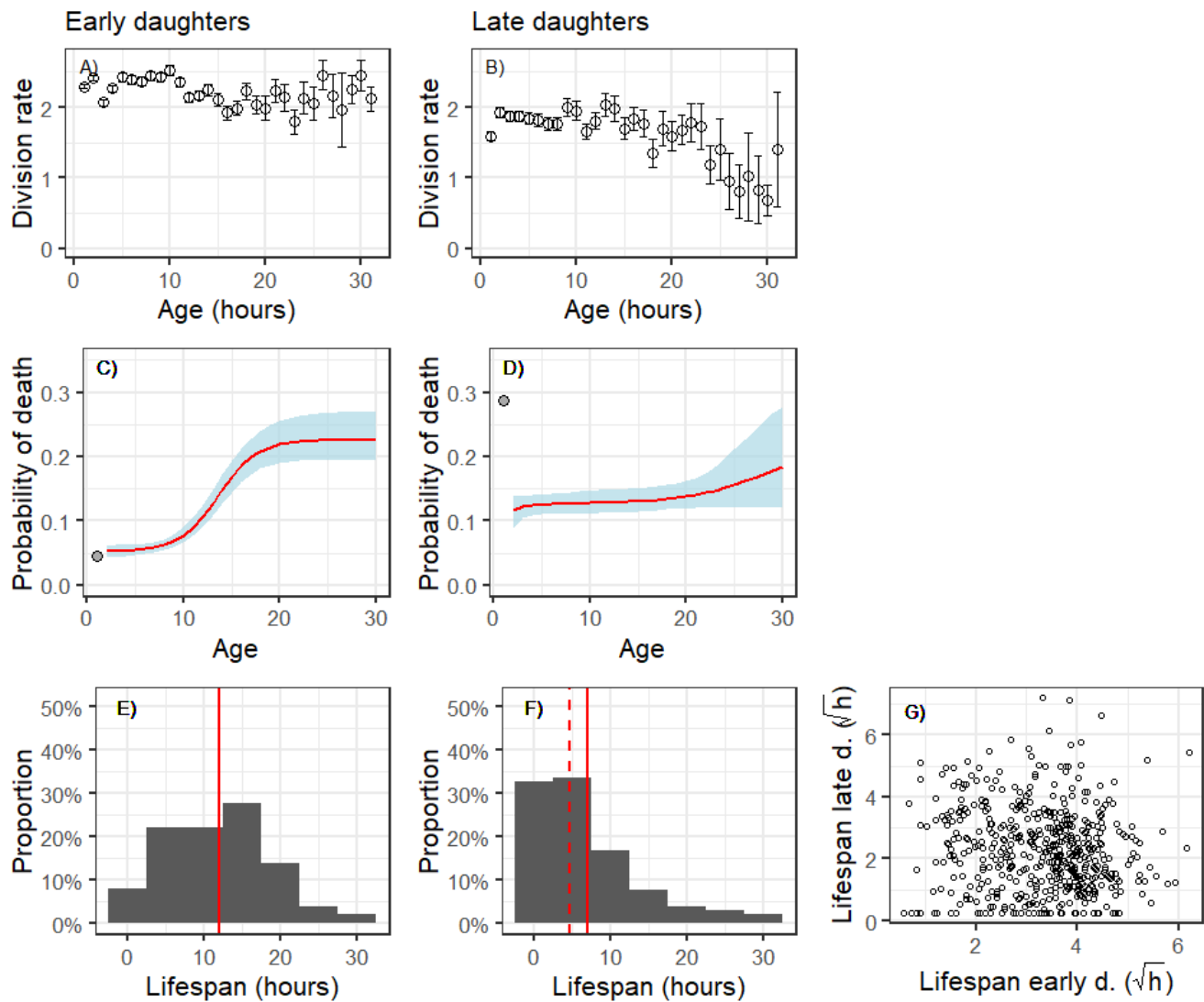149
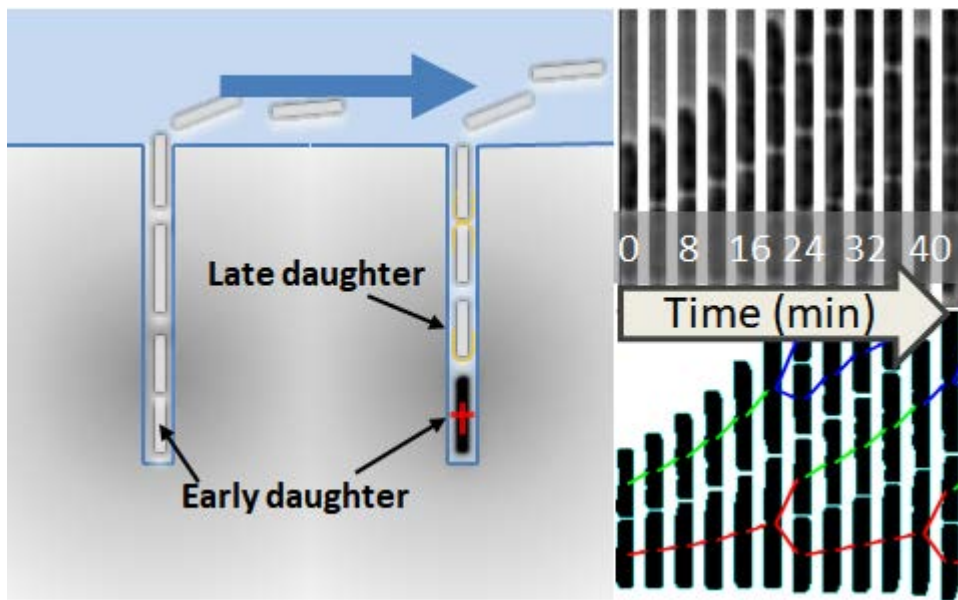
Fig. 1: Left panel: Overview sketch of the microfluidic device with dead-end side channels and the main laminar flow channel where the media is flushed through. The early daughters (founding initial loaded mothers) are the bottommost cells of the dead-end channels. Their daughters (new pole progenitor cells) are located closer to the main laminar flow channel and have more recent poles. When the mother (early daughter) dies (side channel on the right), its last daughter (1st generation late daughter) is then tracked throughout its life. Accordingly, 2nd generation late daughter cells are tracked once their mother (1st generation late daughter) dies. Right top and bottom panel: Phase contrast time sliced (4 min intervals) side channel images with initial loaded early daughter at the bottom (old pole progenitor). Growth (cell elongation) and division can be tracked throughout their life as depicted in the segmented cell lineages (bottom right panel). See also movie S1.

Results and Discussion

Chronological aging in *E. coli*

8

164   In our experiments, we followed by automated time-lapse microscopy 516 early daughters throughout

165   their lives as they divide and age in microfluidic dead-end channels (Fig. 1). We also followed two

166   generations of late daughters of these 516 early daughters and recorded each cells growth rate and

167   lifespan. In this, we reveal classical senescence patterns of a decrease in reproduction (Fig. 2A, B) —

168   indicated by decreased cell elongation and increased size at division with age (Fig. S2, Table S1) — for

169   both early and late daughters (Figure 2A, B). The observed senescence patterns (Fig. 2C, D) describe

170   chronological aging in *E. coli* and support previous studies on replicative senescence (time counted as

171   number of divisions) in this species (Lindner et al. 2008, Wang et al. 2010) (Fig. S2 & Fig. S4). The

172   main result highlights that early daughters and late daughters differ fundamentally in their senescence

173   pattern, even though they are isogenic and grown in a highly controlled environment. Only the early

174   daughters exhibit the classical senescence pattern, marked by an early exponential increase of the

175   probability of death followed by a later age mortality plateau. Late daughters have the same probability

176   of death across most of their lives, i.e. no senescence is observed at the population level. Only late in life

177   does mortality increase, but this increase is largely driven by only one data point, the one for the last age

178   class (>30h) and is accompanied by increased uncertainty due to small sample size at that age. Such a

179   plateau, exhibited by the early daughters — recurrent in many higher organisms including humans

180   (Vaupel et al. 1998) — has not been previously shown for bacteria, potentially indicating deep-rooted

181   features of aging and senescence. In yeast, ambiguous results on senescence patterns have been described

182   (Minois et al. 2005, Denoth Lippuner et al. 2014).

Fig. 2: Division rate (divisions per hour) (A, B) and probability of death per hour (C, D) with increasing age, as well as lifespan distribution (in hours) (E, F) of isogenic *E. coli* cells grown under highly controlled environmental conditions in a microfluidic device (Fig. 1, movie S1). Age patterns are shown for early daughters (A, C, E; N=516), and late daughters (B, D, F; N=516). Late daughters are the last offspring of the founding early daughters. The correlation of early daughter's lifespan (mothers' lifespan) (square root transformed for better visibility; N=516) versus the lifespan of their last daughter cell (late daughter cells; N=516) is shown in panel (G). For (A, B) hourly means ± standard errors are plotted, for

191   (C, D) the fitted regression ± 95% confidence intervals are plotted (confidence intervals are estimated

192   based on individual level data SI1). The fitted regression (red lines) are likelihood optimization for

193   Gamma-Gompertz-Makeham functions and relate closely to the modeling approach we took below (C,

194   D, see also Fig. 3, simulations below, and SI1; Table S1, Table S2 for statistical testing) (Burnham and

195   Anderson 1998). The grey points in panel C, D, mark average first hour probability of death which have

196   been excluded from the modeling. For lifespan distributions (E, F), mean and median are marked by solid

197   and dashed lines respectively. For patterns of the second generation late daughters, see Table S2, Table

198   S3, Table S4, and Fig. S3, Fig. S7, Fig. S8, Fig. S9, Fig. S10, Fig. S11.

199

200   The probability of death of newborn late daughters (<=1hour, filled grey data point in Fig. 2D) drops

201   after the first hour to a level that is lower than their long-lived mothers (early daughters above age 20)

202   and then remains at that level throughout their lives. This drop in mortality early in life of late daughters

203   suggests a damage purging effect (see below). Such a drop of mortality after birth might indicate

204   heterogeneity among newborns amenable to evolutionary selective forces (Yashin et al. 1994), e.g.

205   heterogeneity in maternally-transmitted damage between mothers and daughters. With increasing age we

206   detected increased variance and increased uncertainty of parameter estimation (Fig. 2 A-E). Such

207   increase is expected for age-structured demographic analyses and well understood for its declining

208   number of individuals with age (Brillinger 1986, Klein and Moeschberger 2003, Scherbov and Ediev

209   2011). The increase in variance is more pronounced for probabilities of death (Fig. 2 C, D) than for

210   division rates (Fig. 2 A, B), because each individual dies only once while each individual divides multiple

211   times throughout its life and hence division rates suffer less from smaller sample sizes. Binning over

212   larger time spans or having an earlier open age bracket would diminish the effect of increased variance

213   with age.

214

215   Damage accumulation and selection

216   If we assume, as in most physiological theories of aging, that accumulated damage is the determining

217   factor for the probability of death, then the observed constant probability of death with age for older early

218   daughters and the late daughters (Fig. 2C, D) indicates an equilibrium distribution of damage among

219   individuals. Such equilibrium is realized at the population level while the individuals accumulate damage

220   in a stochastic manner. It equilibrates on one hand the accumulation of new damage within individuals

221   similar to processes described by random deterioration models (Weitz and Fraser 2001), and on the other

222   hand, the intracellular repair of damage and purging of damage by two mechanisms. The first mechanism

223   reduces damage within an individual by asymmetric division of damage at cell fission, which increases

224   variance in damage among individuals (mother and daughters). The second mechanism selects against

225   highly damaged cells, i.e. the most damaged cells of a population die, which lowers the average level of

226   damage in the surviving population, and reduces the variance of damage among individuals (Evans and

227   Steinsaltz 2007). Intriguingly, this equilibrium (plateau level) is lower for late daughters (Fig. 2D, see

228   Table S3) than the late-age mortality plateau of the early daughters (Fig. 2C). This indicates — based on

229   fixed frailty models (Missov and Vaupel 2015) — higher heterogeneity in transmitted damage of late

230   daughters compared to early daughters. Such increased heterogeneity at birth predicts an earlier onset of

231   selection against highly damaged cells which would explain why in our simulations (below) late

232   daughters have on average less damage compared to early daughters at the plateau (see Fig. 3A, B, Fig.

233   S10). Purging of damage through asymmetric division at cell fission has been shown in yeast, where late

234   daughters showed reduced lifespan, but through further division and presumably damage dilution, the

235   descendants of these late daughter yeast cells recovered high longevity (Kennedy 1994). This is also

12

236   reminiscent of asymmetric partition of protein aggregates in bacterial cells due to their passive

237   accumulation in bacterial mother cells (Lindner et al. 2008, Coquel et al. 2013).

238

239   Stochastic variability in lifespan and lack of mother-daughter correlation of lifespan

240   We did not find any influence of the lifespan of the mothers on the lifespan of their (last) daughters (Fig.

241   2G) (Table S6, Fig. S8). Since we are working with an isoclonal population we do not expect any genetic

242   variability among mother-daughter pairs; therefore, we would not expect a genetically driven mother-

243   daughter correlation of lifespan caused by additive genetic differences. However, non-genetic factors

244   such as maternal transmitted damage would predict mother-daughter correlated lifespans except if i)

245   daughters would be perfectly rejuvenated — all daughters would be born without damage (see also Fig.

246   3E) —, or ii) if the transmission of damage to the daughter is independent of the amount of accumulated

247   damage by the mother — the mother-daughter transmission of damage is stochastic. Since late daughters

248   display higher probability of death from birth onwards (Fig. 2D), which is indicative of some maternally

249   transmitted damage and obviously shows that late daughters are not perfectly rejuvenated, we can

250   exclude the first explanation why a mother-daughter correlation of lifespan is lacking. This leaves the

251   second explanation where the amount of damage transmitted from the mother to the daughter is stochastic

252   and independent of the age of the mother. Early daughters seem to hold little or no damage at birth, since

253   their mothers have not yet accumulated much damage, whereas the average late daughter seems to be

254   born with some damage that raises its probability of death. The lack of a mother-daughter correlation of

255   lifespan is also remarkable as it contrasts heritability of lifespan in humans and other complex organisms

256   that show similar senescence patterns (Finch and Kirkwood 2000).

257

258   The lack of correlation between mother-daughter lifespan suggests that the assumed mother-daughter

259   transmission of damage is predominantly stochastic. If damage accumulates stochastically within a cell

260   over its life, long-lived mothers might have been lucky and accumulated damage at a lower rate than the

261   average mother, but they still accumulate damage with increasing age. At age of death, long-lived

262   mothers might have similar damage levels compared to short lived mothers. Short-lived mothers, which

263   likely accumulated damage at an exceptional high rate, do not produce daughters with shorter life

264   expectancy. Despite their difference in lifespan, neither long-lived nor short-lived mothers tend to

265   transmit higher or lower amounts of damage to their daughters, otherwise we would find a negative or

266   positive correlation in mother-daughter lifespan (Fig. 2G). Therefore, our observation that early

267   daughters — which are assumed to hold little or no damage at birth — die at very different ages indicates

268   that the process of damage accumulation within an individual appears to be stochastic and varies highly

269   among individuals. Despite an isogenic population in a highly controlled homogeneous environment, we

270   observe a high variation in lifespan and reproduction among individuals, both for early daughters

271   (Median±stdev lifespan 12 ± 7 hours, Coefficient of Variation, CV 0.57, Fig. 2E) (Fig. S7) and late

272   daughters (Median±stdev 5 ± 7; CV=1.01, Fig. 2F). Such high variation supports substantial influences

273   of stochastic events in shaping lifespan.

274

275   <u>Modeling damage accumulation and asymmetric transmission of damage</u>

276   To support our conclusions based on the empirical results and to gain a better understanding of the

277   underlying stochastic processes that shape our observed senescence patterns, we extended random

278   deterioration process models (e.g. random accumulation of damage, see details in Methods and SI1) (Le

279   Bras 1976, Yashin et al. 1994, Evans and Steinsaltz 2007). Our extended model assumes that all cells

280   accumulate damage unidirectionally at the same rate, i.e. cells move with equal probability to a higher

14

281   damage state, mortality increases exponentially with accumulated damage, and each cell suffers from an

282   age-independent baseline mortality risk. We also assume that early daughters are born without damage

283   (Fig. 3A). The results of our simulations show that with increasing age population level damage (and

284   variance) slowly increases at early ages, accelerates after 10 hours and plateaus after 20 hours (Fig. 3A).

285   These patterns in damage accumulation mirror the observed mortality patterns (Fig. 2C). Mortality

286   plateaus, as observed for early daughters, can be explained by either fixed frailty, i.e. heterogeneity in

287   damage stage at birth, or acquired heterogeneity throughout life (Vaupel and Yashin 1985, Yashin et al.

288   1994, Weitz and Fraser 2001, Missov and Vaupel 2015). In our system heterogeneity in damage stage at

289   birth seems to have little influence, at least for early daughter cells. Senescence is driven by an age

290   independent baseline mortality and accrued damage as in random deterioration models (Le Bras 1976,

291   Yashin et al. 1994, Weitz and Fraser 2001). This conclusion is supported by two results of our model.

292   First, most early daughters die with no or very little damage (Fig. S10), and second, the observed survival

293   patterns follow closely the survival curve of simulated cells that did not accumulate any damage

294   throughout life (Fig. 3C).

295

296   Contrasting the assumption for the early daughter cells, in our simulation the average simulated late

297   daughter is born with some damage (~24% are born without damage) (Yashin et al. 1994)(Fig. 3B). For

298   the following results, it is important to note that this heterogeneity in damage at birth of late daughters is

299   an underestimation since we do not include the exceptionally high first-hour mortality rate (grey filled

300   data point in Fig. 2D) for the simulations. In our simulations the distribution of this damage at birth of

301   the late daughters is related to the distribution of the accumulated damage at death of the early daughter

302   cells (mothers of the late daughters, Fig. S10). For the simulations, we assumed that the mother to

303   daughter transmission of damage is a fixed fraction of all the damage the mother accumulated over her

15

304   lifespan. Note, we only simulated a single binomial division, rather than multiple asymmetric fissions as

305   others have done (Evans and Steinsaltz 2007). We computed the fixed fraction of damage transmission

306   between mother and daughter by optimizing the survival pattern predicted by the simulations to the

307   observed survival curves.

308

309   We found that the optimal (simulated) fixed fraction was at a low level of 0.07. This indicates a highly

310   asymmetric division of damage between mothers and daughters. If damage transmission between

311   mothers and daughters would be symmetrical (0.5), the predicted survival of the simulations (Fig. 3D

312   hatched line) does not match the observed survival (Fig. 3D red line). For early daughters, the level of

313   asymmetry makes little difference because most of them die with no or little accumulated damage (Fig.

314   3C, Fig. S10). The predicted survival pattern of late daughters at older ages slowly converges to the

315   simulated survival patterns of undamaged cells (outer right grey line) (Fig. 3D). Therefore, many cells

316   in our simulation that survive to old ages hold little damage, which supports our interpretation of our

317   experimental data that late daughter cells are born with diverse damage states, highly damaged cells are

318   selected against, and at old ages, population-level survival patterns are strongly influenced by cells that

319   have not accumulated much damage.

320

321   Similar selective effects have been described by population level demographic theories as

322   heterogeneity's ruses, where selection among different damage stages (fixed frailty; i.e. heterogeneity in

323   damage stage at birth) leads to diverse senescence patterns at the population level (Vaupel and Yashin

324   1985). Compared to our simple model that only considers a single binary fission (branching) and suggests

325   a strong asymmetry, more complex and realistic models that include multiple branching (fission) events

326   show less extreme asymmetry at cell fission to be adaptive (Evans and Steinsaltz 2007). This difference

16

327   in optimal asymmetry between our simple and the more complex models can be understood in that the

328   asymmetric transmission of damage is distributed over multiple fissions in the more complex models,

329   while for our model it is concentrated at a single event. Even though the optimized fixed transmission

330   fraction between mother and daughters of our model is low at 0.07, such a fixed fraction would lead to a

331   correlation in lifespan between mother and daughters of about 0.25 (Fig. 3E). If different levels of fixed

332   transmissions are simulated, correlation in lifespan between mother and daughters increases with

333   increasing transmission. Only when there is no transmission of any damage (perfect rejuvenation of the

334   daughters) we see no correlation in lifespan (Fig. 3E). The observed data does not support such

335   correlation in lifespan (Fig. 2G), but also does not support perfect rejuvenation (Fig. 2C and D). Hence

336   these simulations support our conclusion that the fraction of transmitted accumulated damage from

337   mother to daughter at cell fission varies stochastically and is not fixed at a low level of 0.07 as our model

338   assumes.

339

340

341
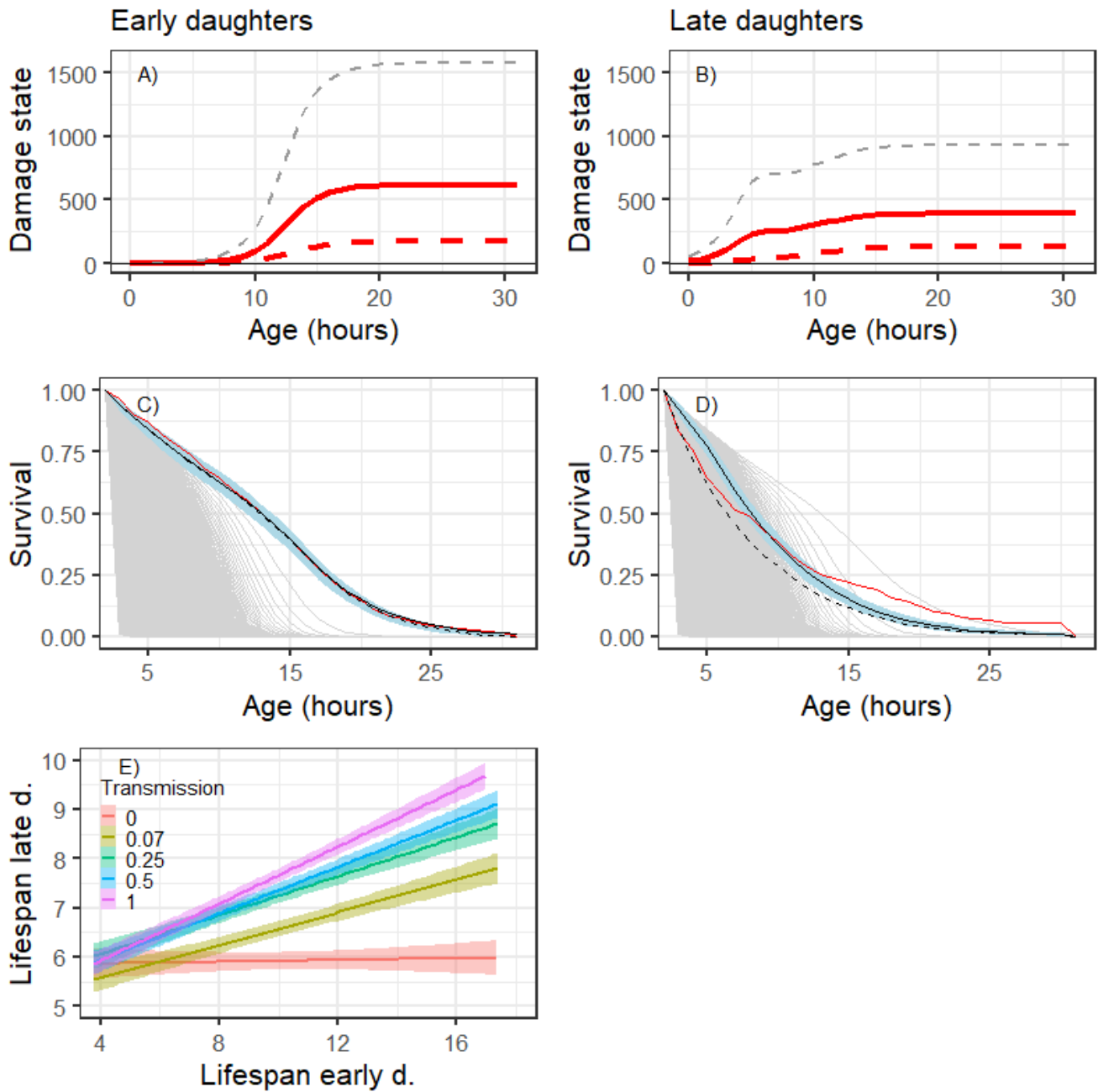
Fig. 3: Random deterioration model: Simulation results are shown of mean (red solid line, + SD grey hatched lines) and median (red hatched line) damage state with increasing age (A, B); observed experimental population level survival curves (red solid line; see also related probability of death Fig. 2

345 C, D and related observed distributions of death Fig. 2E, F), Gamma-Gompertz-Makeham simulated

346 survival curves with symmetric damage transmission (hatched black line) as well as simulated

347 asymmetric damage transmission of 7% (solid black lines ± 95% CI in blue) (C, D). Graphs are shown

348 for early daughter cells (A, C) and late daughter cells (B, D). Thin grey lines in (C, D) depict expected

349 survival curve of simulated cells with different fixed damage state: outermost (right) curve depicts the

350 highest survival of simulated cells with no damage throughout their lives, most left survival curve depicts

351 the lowest survival of simulated cells that were born with maximum damage level of 5000. Lifespan

352 (square root transformed) of simulated 516 early daughter cells (mothers) versus the lifespan of their

353 simulated last daughter cell (late daughter cells) with different levels of mother to daughter damage

354 transmission (E). The different scenarios include the optimized fixed transmission level at 0.07 (forest

355 green), a scenario for perfect rejuventation, i.e. 0 transmission (red), 0.25 transmission (green), 0.5

356 transmission, i.e. symmetric (equal) transmission between mother and daughter (blue), and transmission

357 of all accumulated damage to the daughter (1) (pink).CI are shown for each correlation in lifespan

358 between mothers and daughters as shaded areas.

359

360 In this study, our experimental setup limits our analysis to two extreme cases: early and late daughter

361 cells (in fact the last daughter cells). We hypothesize that the results do not only hold for these two

362 extremes but rather portray the extremes of a continuous process across different aged cells. Two

363 observations support our claim: first, changes in mortality of early daughters (Fig. 2C) and age patterns

364 in reproduction (Fig. 2A) are somewhat gradual (more so for survival than for reproduction), suggesting

365 a gradual underlying mechanism; second, we do not observe a pronounced pattern just before death (Fig.

366 S5 & Fig. S6, Table S5). Such a pattern would be expected if the last daughters are exceptional because

19

367   their mothers are approaching death, for instance in the way as predicted under terminal investment

368   theories (Clutton-Brock 1984).

369

370   <u>Two stochastic processes shape diverse senescence patterns</u>

371   We conclude that the diverse senescence patterns, including the classical senescence pattern of a

372   mortality plateau, are determined by two stochastic processes that relate to underlying (damage) states

373   and only indirectly to age (Yashin et al. 1994, Wachter 1999, Weitz and Fraser 2001, Evans and Steinsaltz

374   2007). The primary process is a random deterioration process, e.g. the stochastic accumulation of damage

375   throughout life, and the secondary process involves the stochastic transmission of damage from the

376   mother to their daughters at cell fission. This transmitted damage or some other unknown aging factor

377   increases the probability of death but is "non-heritable" as we show by the lack of correlation between

378   mother and daughter lifespan (Yashin et al. 1994, Wachter 1999, Weitz and Fraser 2001, Evans and

379   Steinsaltz 2007). Not only additive genetic variation but also other commonly assumed drivers of

380   senescence, such as epigenetic variability, age itself, or the (extrinsic) environment can be ruled out as

381   major players in our study. If epigenetic variability had a significant influence, a positive correlation

382   among mother and daughter lifespan would be seen. If chronological age determined senescence, early

383   and late daughter cells would show similar mortality patterns, hence senescence is rather driven by stage

384   dynamics than by chronological age. The highly controlled microfluidic system creates a uniform

385   environment and hence we can exclude extrinsic environmental drivers; this does not imply that

386   senescence patterns do not differ under different environmental conditions, we just investigated only one

387   specific environment. For instance, under complex media variance in division size and related division

388   rate is increased compared to the minimum medium we used (Gangan and Athale 2017). Minimum

389   medium also decreases the rate of filamentation, a stress response that causes continued cell elongate

390   without dividing. Recovery of filamentous cells is rarely observed under minimum medium but frequent

391   under complex medium (Wang et al. 2010) (see also SI). The near identical conditions cells experience

392   in the microfluidic system decreases environmental variability compared to naturally experienced micro-

393   habitats. The laminar flow provides large amounts of fresh media that constantly diffuses within seconds

394   into the dead-end side channels and therefore prohibits built-up of micro-environmental-niches. Though,

395   such micro-environments (e.g. biofilms) are characteristic for the natural conditions in the guts of the

396   mammalian hosts most *E. coli* life and have evolved under. The microfluidic system we use largely

397   prevents cell-to-cell contact and chemical communication among cells that can influence population

398   growth (Aoki et al. 2005). The highly controlled conditions therefore lowers phenotypic variability

399   compared to natural conditions. To what degree senescence patterns are altered by the environment

400   remains to be explored. Temperature seem to conserve the shape of senescence patterns and simply scales

401   patterns differently, whereas nutrient concentrations and nutrient source might alter shapes as has been

402   found in other organisms (Stroustrup et al. 2016)(Steiner unpublished).

403

404   Our findings indicate that two simple stochastic processes can create complex senescence patterns. Easily

405   understood, simplistic, and plausible arguments behind evolutionary theories of aging might lure readers

406   into the misconception that chronological age in itself plays an important role in senescence. Such

407   simplistic assumptions of age-specific drivers must be approached with caution and seem not applicable

408   to this study. Selective forces likely decline with time in our system, but the decline might be dominated

409   by underlying stage dynamics. Selection on heterogeneity among individuals is rather generated by such

410   stage dynamics than by increasing chronological age. In this sense, selective forces and their decline vary

411   considerably among individuals, even though genetic load that relates to the accumulation of deleterious

412   mutations should be negligible in an isoclonal population as ours. The substantial effect of stochastic

413 events on life histories is also indicated by the large variability in life histories despite excluding any

414 genetic or environmental variability. Such large stochastic variation supports arguments behind neutral

415 theories of life history (Steiner and Tuljapurkar 2012) that suggest that stochastic variability can account

416 for substantial fractions of the total variability in fitness components. Our interpretation of stochastic

417 events determining individual life courses is consistent with findings of significant stochastic influences

418 at the molecular (Elowitz et al. 2002) and protein level (Tyedmers et al. 2010, Balázsi et al. 2011) and

419 adds to the growing interest in such phenotypic heterogeneity and individuality (Wolf et al. 2007,

420 Davidson and Surette 2008, Ackermann 2015).

421

422 Future challenges will include determining whether these stochastic processes are neutral or adaptive,

423 and what drives their evolution (Steinsaltz and Evans 2004, Kærn et al. 2005, Norman et al. 2015, Vera

424 et al. 2016). For the basic aging processes that drive senescence, the causal relationships that drive age

425 patterns are currently unknown (Lindner and Demarez 2009, López-Otín et al. 2013). The complex

426 senescence patterns found in this study of a simple model organism under highly controlled conditions

427 emphasizes the challenges to quantify contributions of well-defined determinants of aging in the complex

428 systems on which most aging research is focused (López-Otín et al. 2013). Comparing mean

429 characteristics of differently aged individuals as frequently done in aging research might hold limited

430 insights in system where determining stages are likely highly dynamic. In light of the growing evidence

431 that stochastic processes can have cascading effects across all levels of higher organisms (Finch and

432 Kirkwood 2000, Elowitz et al. 2002, Balázsi et al. 2011) new avenues in aging research may require a

433 shift towards the underlying stochastic processes that drive such stage dynamics in simple systems like

434 bacteria and perhaps beyond. Identifying the underlying currently unknown (damage) states remains

435 another challenge that we believe requires a combined quantitative demographic and mechanistic

22

436   approach, because of the high level of stochastic influences. Promising steps in such directions have been

437   initiated by theoretically exploring stage-specific alleles shaping senescence patterns (Wachter et al.

438   2014) and by exploring transcription factor signal dynamics at the single cell level across increasing parts

439   of the lifespans of many individuals (Norman et al. 2013).

440

441

442

443   **Acknowledgements**

446

447   **References**

448   Ackermann, M. 2015. A functional perspective on phenotypic heterogeneity in microorganisms. - Nat.
449   Rev. Microbiol. 13: 497–508.
450   Ackermann, M. et al. 2003. Senescence in a bacterium with asymmetric division. - Science 300: 1920.
451   Ackermann, M. et al. 2007. On the evolutionary origin of aging. - Aging Cell 6: 235–44.
452   Aoki, S. K. et al. 2005. Contact-Dependent Inhibition of Growth in Escherichia coli. - Science (80-.).
453   in press.
454   Balázsi, G. et al. 2011. Cellular decision making and biological noise: from microbes to mammals. -
455   Cell 144: 910–925.
456   Blattner, F. R. 1997. The Complete Genome Sequence of Escherichia coli K-12. - Science (80-.). 277:
457   1453–1462.
458   Brillinger, D. R. 1986. A Biometrics Invited Paper with Discussion: The Natural Variability of Vital
459   Rates and Associated Statistics. - Biometrics 42: 693.
460   Burnham, K. and Anderson, D. R. 1998. Model selection and multimodel inference : a practical
461   information-theoretic approach. - Springer.
462   Caswell, H. 2001. Matrix population models: construction, analysis, and interpretation. - Sinauer
463   Associates.
464   Charlesworth, B. 1994. Evolution in age-structured populations. - Cambridge University Press.
465   Clutton-Brock, T. 1984. Reproductive effort and terminal investment in iteroparous animals. - Am.
466   Nat. 123: 212–229.
467   Coquel, A.-S. et al. 2013. Localization of protein aggregation in Escherichia coli is governed by

468   diffusion and nucleoid macromolecular crowding effect. - PLoS Comput. Biol. 9: e1003038.

469   Coulson, J. C. and Fairweather, J. A. 2001. Reduced reproductive performance prior to death in the

470   Black-legged Kittiwake: senescence or terminal illness? - J. Avian Biol. 32: 146–152.

471   Davidson, C. J. and Surette, M. G. 2008. Individuality in Bacteria. - Annu. Rev. Genet. 42: 253–268.

472   Denoth Lippuner, A. et al. 2014. Budding yeast as a model organism to study the effects of age. -

473   FEMS Microbiol. Rev. 38: 300–25.

474   Elowitz, M. B. et al. 2002. Stochastic gene expression in a single cell. - Science (80-.). 297: 1183–

475   1186.

476   Evans, S. N. and Steinsaltz, D. 2007. Damage segregation at fissioning may increase growth rates: a

477   superprocess model. - Theor. Popul. Biol. 71: 473–90.

478   Finch, C. and Kirkwood, T. B. 2000. Chance, Development, and Aging. - Oxford University Press.

479   Gangan, M. S. and Athale, C. A. 2017. Threshold effect of growth rate on population variability of

480   Escherichia coli cell lengths. - R. Soc. open Sci. 4: 160417.

481   Gasset-Rosa, F. et al. 2014. Direct assessment in bacteria of prionoid propagation and phenotype

482   selection by Hsp70 chaperone. - Mol. Microbiol. 91: 1070–87.

483   Hamilton, W. D. 1966. The moulding of senescence by natural selection. - J. Theor. Biol. 12: 12–45.

484   Jagers, P. 1978. Balanced exponential growth: what does it mean and when is it there? - In:

485   Biomathematics and cell kinetics. Elsevier, pp. 21–29.

486   Johnson, L. R. and Mangel, M. 2006. Life histories and the evolution of aging in bacteria and other

487   single-celled organisms. - Mech. Ageing Dev. 127: 786–93.

488   Jones, O. R. et al. 2014. Diversity of ageing across the tree of life. - Nature 505: 169–73.

489   Jouvet, L. et al. 2017. Demographic variability and heterogeneity among individuals within and among

490   clonal bacteria strains. - Oikos in press.

491   Kærn, M. et al. 2005. Stochasticity in gene expression: from theories to phenotypes. - Nat. Rev. Genet.

492   6: 451–464.

493   Kennedy, B. K. 1994. Daughter cells of Saccharomyces cerevisiae from old mothers display a reduced

494   life span. - J. Cell Biol. 127: 1985–1993.

495   Kirkwood, T. B. L. 2005. Understanding the odd science of aging. - Cell 120: 437–47.

496   Kirkwood, T. B. L. et al. 2005. What accounts for the wide variation in life span of genetically identical

497   organisms reared in a constant environment? - Mech. Ageing Dev. 126: 439–443.

498   Klein, J. P. and Moeschberger, M. L. 2003. Survival analysis : techniques for censored and truncated

499   data. - Springer.

500   Le Bras, H. 1976. Lois de mortalité et age limite. - Population (Paris). 33: 655–691.

501   Lindner, A. B. and Demarez, A. 2009. Protein aggregation as a paradigm of aging. - Biochim. Biophys.

502   Acta 1790: 980–96.

503   Lindner, A. B. et al. 2008. Asymmetric segregation of protein aggregates is associated with cellular

504   aging and rejuvenation. - Proc. Natl. Acad. Sci. U. S. A. 105: 3076–81.

505   López-Otín, C. et al. 2013. The hallmarks of aging. - Cell 153: 1194–217.

506   Mattick, K. et al. 2003. Morphological changes to Escherichia coli O157:H7, commensal E. coli and

507   Salmonella spp in response to marginal growth conditions, with special reference to mildly

508   stressing temperatures. - Sci. Prog. 86: 103–113.

509   Medawar, P. B. 1952. An unsolved problem of biology. - In: Uniqueness of the Individual. H. K.

510   Lewis, in press.

511   Minois, N. et al. 2005. Advances in measuring lifespan in the yeast Saccharomyces cerevisiae. - Proc.

512   Natl. Acad. Sci. U. S. A. 102: 402–6.

24

513 Missov, T. I. and Vaupel, J. W. 2015. Mortality Implications of Mortality Plateaus. - SIAM Rev. 57:
514   61–70.
515 Norman, T. M. et al. 2013. Memory and modularity in cell-fate decision making. - Nature 503: 481–
516   486.
517 Norman, T. M. et al. 2015. Stochastic Switching of Cell Fate in Microbes. - Annu. Rev. Microbiol. 69:
518   381–403.
519 R Core Team, R. A. language and environment for statistical computing. 2016. R: A language and
520   environment for statistical computing. (RDC Team, Ed.). - R Found. Stat. Comput. 1: 409.
521 Scherbov, S. and Ediev, D. 2011. Significance of life table estimates for small populations: Simulation-
522   based study of estimation errors. - Demogr. Res. 24: 527–550.
523 Steiner, U. K. and Tuljapurkar, S. 2012. Neutral theory for life histories and individual variability in
524   fitness components. - Proc. Natl. Acad. Sci. U. S. A. 109: 4684–9.
525 Steinsaltz, D. and Evans, S. N. 2004. Markov mortality models: implications of quasistationarity and
526   varying initial distributions. - Theor. Popul. Biol. 65: 319–37.
527 Stewart, E. J. et al. 2005. Aging and death in an organism that reproduces by morphologically
528   symmetric division. - PLoS Biol. 3: e45.
529 Stroustrup, N. et al. 2016. The temporal scaling of Caenorhabditis elegans ageing. - Nature 530: 103–
530   107.
531 Tyedmers, J. et al. 2010. Cellular strategies for controlling protein aggregation. - Nat. Rev. Mol. cell
532   Biol. 11: 777–788.
533 Vaupel, J. W. and Yashin, A. I. 1985. Heterogeneity's Ruses: Some Surprising Effects of Selection on
534   Population Dynamics. - Am. Stat. 39: 176.
535 Vaupel, J. W. et al. 1998. Biodemographic Trajectories of Longevity. - Science (80-.). 280: 855–860.
536 Vaupel, J. W. et al. 2004. The case for negative senescence. - Theor. Popul. Biol. 65: 339–351.
537 Vera, M. et al. 2016. Single-Cell and Single-Molecule Analysis of Gene Expression Regulation. -
538   Annu. Rev. Genet. 50: 267–291.
539 Wachter, K. W. 1999. Evolutionary demographic models for mortality plateaus. - Proc. Natl. Acad. Sci.
540   96: 10544–10547.
541 Wachter, K. W. et al. 2014. Evolutionary shaping of demographic schedules. - Proc. Natl. Acad. Sci. U.
542   S. A. 111 Suppl: 10846–53.
543 Wang, P. et al. 2010. Robust growth of Escherichia coli. - Curr. Biol. 20: 1099–103.
544 Weitz, J. and Fraser, H. 2001. Explaining mortality rate plateaus. - Proc. Natl. Acad. Sci. U. S. A. 98:
545   15383–15386.
546 Williams, G. C. 1957. Pleiotropy, Natural Selection, and the Evolution of Senescence. - Evolution (N.
547   Y). 11: 398.
548 Williams, G. C. 1966. Adaptation and natural selection : a critique of some current evolutionary
549   thought. - Princeton Univeristy Press.
550 Wolf, M. et al. 2007. Life-history trade-offs favour the evolution of animal personalities. - Nature 447:
551   581–584.
552 Yashin, A. I. et al. 1994. A duality in aging: the equivalence of mortality models based on radically
553   different concepts. - Mech. Ageing Dev. 74: 1–14.

554

555 **Supporting information SI1**

556

557 **Strains and growth conditions**

558 We fabricated the microfluidics chips as previously described (Gasset-Rosa et al. 2014). We grew *E. coli*

559 K12 MG1655 (Blattner 1997) strain derivative (intC::pSulA-yfp) cells at 43°C in filtered minimal

560 medium supplemented with 0.4% Glucose and 0.2% Casamino Acids (hereafter M9). We diluted 100µl

561 of the overnight culture into 50ml of M9 and then grew it at 43°C to exponential growth phase (OD600

562 ~0.2). We centrifuged the cells and resuspended the cell pellet in 100µl of M9 to load them into the chip

563 by injection into the main (feeding) channel followed by centrifugation (15 minutes at ~168g). We

564 applied a continuous laminar flow (2.7ml/h) of M9 supplemented with 1.5% Polyethylene Glycol (PEG

565 P3015 Sigma Aldrich) through the main channel throughout the experiment. The temperature was kept

566 constant at 43°C (see below).

567

568 **Time-lapse imaging**

569 We followed bacterial growth in the microfluidics chip by phase-contrast time-lapse imaging at a rate of

570 4min/frame using a MetaMorph (Molecular Devices)-controlled inverted Nikon microscope (Eclipse Ti,

571 100xobjective, CoolSNAP HQ2 camera) with a temperature-control chamber (Live Imaging Services).

572 We continuously scanned 44 positions, each comprising 18 channels, for 77 hours, in two independent

573 experimental sets.

574

575 **Image analysis**

576 We used a custom image analysis to segment all cells within the side channels per frame, the software

577 measured the cells' location and size within the time series and generated cell lineages. To this end, phase

578   contrast time-lapse images were lowpass-filtered and background flattened (MetaMorph Molecular

579   Devices software) to increase contrast. We further processed the images by a customized ImageJ plugin

580   for cell segmentation to crop each of the growth channels, stabilize the time sequenced images, adjust

581   the brightness and to create a binary image by thresholding and filtering (median filter). Finally, the

582   ImageJ plugin water-sheds the time sliced images. We then applied a final round of segmentation in

583   Matlab by correcting errors in segmentation by checking for minimum (0.8) and maximum (1.4) cell

584   elongation rates for each cell (size time-4 min, size time+4min). This way, we recorded for any time

585   points (at 4 minute intervals) the exact location of a cell in the side channel (the pixel coordinate of the

586   center of mass of the cell area), the side channel of the cell, and if a cell divided. By the position within

587   the side channel we determined which cell was the mother (old pole progenitor) cell (bottommost cell),

588   their most recent daughter (new pole progenitor) cell and so forth. We measured the length of a cell as

589   the largest distance of the rod shaped cell in the orientation of the side channel. We applied a minimum

590   "cell length" of ~1µm to exclude artefacts originating mainly from small deformations in the growth

591   channels, or some shadows/reflections generated at the dead end of the growth channel.

592

593   **Age at death**

594   We defined age at death as the time when a cell stopped growing and dividing for at least one hour and

595   20 min. None of the cells divided after such a long division arrest or resumed growth.

596

597   **Early and late daughter cells**

598   We defined the early daughter population as the cells that were initially loaded into the microfluidic chip

599   and settled at the dead-end of the side channels. They originated largely from young mothers because the

600   population was in exponential growth phase when we loaded cells into the chip (Jagers 1978). The age

27

601   distribution of these early daughter cells is, because of the exponential growth phase, negatively

602   exponentially distributed. We show their expected age distribution in Fig. S1, based on a Leslie matrix

603   generated from the survival and division rates of the early daughters (Fig. 2A & C). Due to the

604   exponential growth phase, we assume a stable age distribution (the right eigenvector corresponding to

605   the dominant eigenvalue of the Leslie matrix) (Caswell 2001). We tracked these early daughter cells to

606   the end of their lives (Fig. 1, movie S1). The last daughters that were produced by these early daughter

607   cells are the late daughter population. These late daughters are all of age zero but originate from mother

608   cells (the early daughters) that had accumulated damage over their lives, and that were only one division

609   from dying. We again tracked these late daughters throughout their lives. We focus mainly on these first

610   two types of cells (early and late daughters), though as expected, the next generation of late daughter

611   cells (second generation late daughters) follow the late daughter patterns (Fig. S4-6).
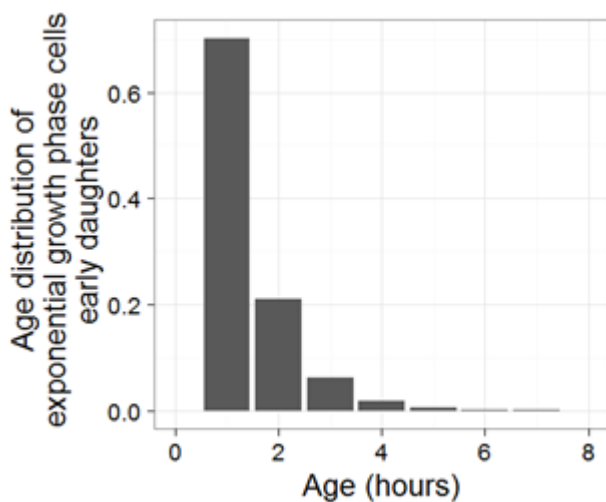
612

613   Fig. S1: Expected (stable) age distribution (in hours) of early daughters (initial loaded cells), estimated

614   from a Leslie matrix parameterized with the demographic rates of the early daughter cells. Due to the

615   theory of stable age populations, the distribution of the ages of the mothers of these early daughters

616   should be exactly as the (stable) age distribution shown here of the initial loaded (early daughter cells)

617   at the start of the experiments.

618

619   **Estimating demographic parameters**

620   Image analysis (see above) provided us the basis for estimating the age-specific demographic parameters:

621   division rate, cell elongation rate, size at division, and survival rate. We excluded all cells that were not

622   tracked throughout their lives. This concerned mostly cells that filamented (cell division arrested without

623   growth arrest) and were flushed out of the side channels when they reached a size longer than 25 µm

624   (length of the side channel). We also excluded all (early and late daughter) cells that died at chronological

625   age 0 (never started to grow or divide). This was practiced because loading into the chip might be

626   damaging and we wanted to exclude such death. This approach was conservative, because fewer early

627   daughters never started growing or divided compared to late daughters (who could not have been

628   damaged by the loading). We used data from 516 early daughters that produced 516 late daughters which

629   in turns produced 298 (second generation) late daughters that were tracked throughout their lives.

630

631   **Statistical analysis**

632   We did the statistical analysis using the R software (R Core Team 2016). We estimated and plotted hourly

633   rates for division rates, cell elongation, and cell size at division rather than rates on the 4 min intervals

634   because data would be sparse for 4 min intervals at older ages. Already the hourly rates at old ages suffer

635   from sparse estimates and increased uncertainty. We also clustered all data of ages beyond 30 h for the

636   same reason. To guide statistical testing, we used model selection (Burnham and Anderson 1998) based

637   on AIC (Akaike Information Criteria) and considered — as common practice —better support between

638   models when the ΔAIC was more than 2. For the parameter estimation of the GGM and extended random

29

639   deterioration models, we used the DEoptim R package and the optim function within the stats R package.

640   We calculated the CI (Fig. 2 C & D) by bootstrapping 1000 times. This bootstrapping is based on

641   individual level data not the hourly means Fig. 2 C, D. We choose such an likelihood based global

642   optimization approach to closely relate to the GGM modeling approach we used for the simulations.

643   Using model comparison (AIC) based on the hourly rates (results not shown) selects for models with

644   sigmoidal shapes like the GGM likelihood optimization, i.e. an early exponential increase in mortality

645   followed by a late age mortality plateau (Fig. 2 C). For early daughters, other exponential or linear

646   functions receive less support. For late daughters model comparisons selected non-senescence (Fig. 2 D,

647   flat mortality) over linear or exponential models. We did not test for any breakpoint models or step

648   functions, since such models are not expected based on evolutionary theories of aging.

649

650   **Lifespan distribution second generation late daughters**

651   In the main article, we focused on early and late daughter cells. Qualitatively, patterns of the second gen

652   eration late daughters (the last daughters produced by the late daughters) correspond to those of their m

653   others (the late daughters), though data becomes sparse uncertainty increases and some deviations occur

654   . Fig. S7 illustrates lifespan distributions of the 298 second generation late daughters, their mothers (late

655   daughters), and grandmothers (early daughters). Kolmogorov-Smirnov tests (two-sided) verifies that bo

656   th lifespan distributions between early and late daughters ($D = 0.3691$, $p < 0.00001$), and early to secon

657   d generation late daughters are significantly different ($D = 0.4094$, $p < 0.00001$), while those between la

658   te daughters and second generation late daughters do not differ ($D = 0.0973$, $p = 0.1189$).
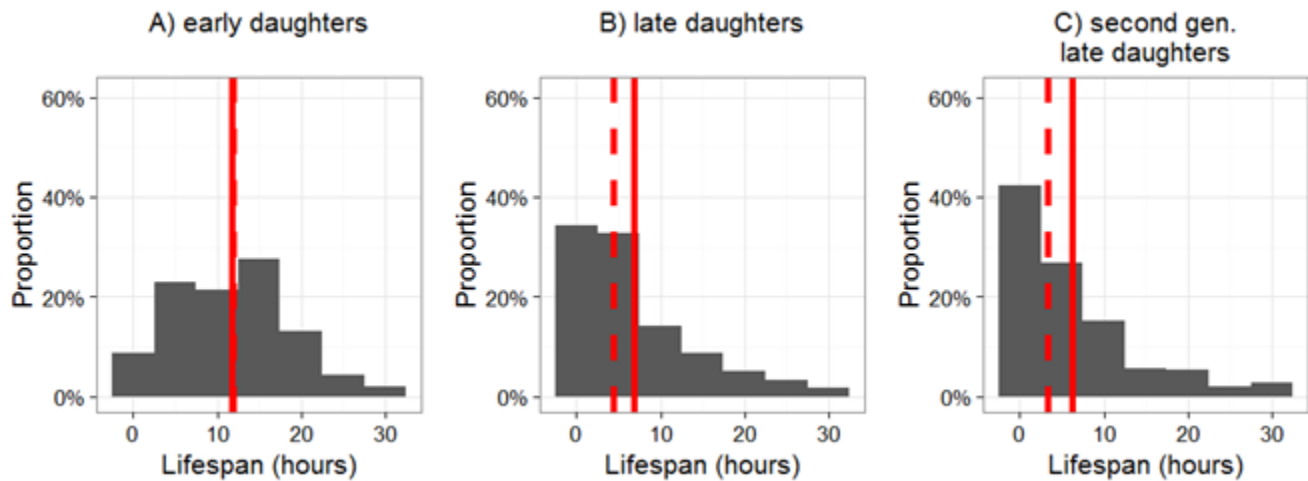
Fig. S7: Lifespan distribution (in hours) of isogenic *E. coli* cells grown under identical environmental conditions in a microfluidic device (Fig. S1). 1A – Founding early daughter cells (Median±stdev lifespan 12 ± 6.8 hours, Coefficient of Variation, CV 0.57) (N=298); 1B – Late daughters (last daughter) of the founding early daughters of 1A (Median±stdev lifespan 4.4 ± 7.0 hours, Coefficient of Variation, CV 1.03) (N=298); 1C – Second generation late daughters (last daughter of the late daughters of 1B; (Median±stdev lifespan 3.4 ± 7.1 hours, Coefficient of Variation, CV 1.14) (N=298). (Fig. S1 & S3). Hence, early daughters are the mothers of late daughters and grandmothers of second generation late daughters.

Heritability or cross generation correlation in lifespan

In order to estimate correlation of lifespan between mother cells (early daughters) and their last (late) daughter cells, we used linear models on square root transformed data for age at death (lifespan) for the mothers' lifespan as response variable and their last daughters' lifespan as explanatory variable, or intercept only models (null model) as comparative models.

675   Model selection (Table S6) does not allow distinguishing between the two alternative models and we ca

676   nnot completely rule out that the longer-lived mothers produce slightly shorter-lived late daughters (Fig

677   . 2G). In any case, the effect size is weak and such a negative correlation would suggest that longer-live

678   d mothers accumulate more damage that is then partly transmitted to their late daughter. Similar results

679   hold for late daughters to second generation late daughters (Fig. S8). We cannot completely rule out a w

680   eak tendency that long-lived (late daughter) mothers produce last daughters (second generation late dau

681   ghters) that live slightly shorter (Table S6). In any case, our simulations with a low fixed transmission r

682   ate of 7% of damage transmitted between mother and daughters would lead to much higher correlation i

683   n lifespan as observed (Fig. 3E main text).

684
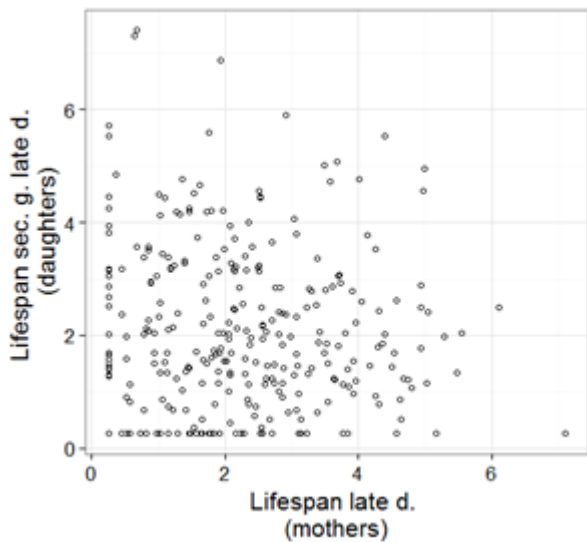
685

686   Fig. S8: Correlation between lifespan (Square root-transformed) of the 298 late daughters [mothers]

687   versus the lifespan of their last daughter cell, the second generation late daughters (Table S6).

688

689   Table S6: Model selection for correlation between lifespan (Square root transformed, Gaussian error)

Model	Slope	Std. Error	T value	p-value	AIC	ΔAIC
Early daughters [516 mothers] and daughter cell (last daughter of early daughter)						

sqrt(Lifespan Daughters) ~ sqrt(Lifespan mothers)	-0.10	0.05	-1.8	0.07	1774.1
sqrt(Lifespan Daughters) ~ intercept only					1775.5	1.3

Late daughters [mothers 298] and second generation late daughters
(last daughter cell produced by late daughters)

sqrt(Lifespan Daughters) ~ sqrt(Lifespan mothers)	- 0.09	0.06	-1.55	0.12	1061.1
sqrt(Lifespan Daughters) ~ intercept only					1061.5	0.4

690

691 **Lifespan and lifetime reproductive success: reproductive and chronological aging**

692 Previous aging studies on *E. coli* (Stewart et al. 2005, Wang et al. 2010) and other bacteria (Ackermann

693 et al. 2003) or many yeast studies (Denoth Lippuner et al. 2014) have focused on replicative aging and

694 patterns have been described for time measured in number of divisions. Such age measures can be

695 difficult to compare directly to chronological age if the time between divisions varies. Nonetheless, we

696 detected a strong correlation between lifespan and the lifetime reproductive success (number of divisions

697 an individual undergoes throughout its life), but there remains some variation, particularly for longer

698 lived individuals (Fig. S4).
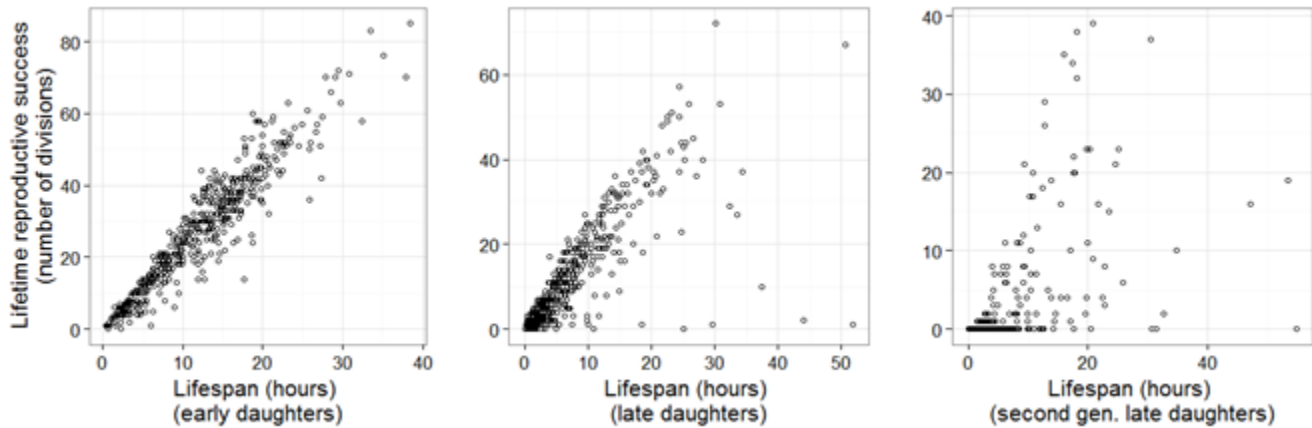
699

700 Fig. S4: Correlation between lifespan and the lifetime reproductive success (cumulative number of

701 divisions an individual undergoes throughout its life) for left panel) the 516 early daughters, mid panel)

702 the 516 late daughters, and right panel) the 298 second generation late daughters.

33

703

Division rate

705 We fitted linear models on hourly average division rates (at the cellular level) as response variable and

706 age as explanatory variable. A model with a linear and quadratic term was best supported for the early

707 (Fig. 2A), late (Fig. 2B) and second generation late (Fig. S3A) daughters (Table S2).

708

709 Table S2: Model selection division rate

Model	Slope±Std. Error	Quadratic term±StdE	AIC	ΔAIC
Early daughters				
Divison rate ~intercept only			19663	24
Divison rate ~age	-0.011±0.002		19642	21
Divison rate ~age+age^2	**0.005±0.0078**	**-0.0007±0.0003**	**19638**	
Late daughters				
Divison rate ~intercept only			12432	24
Divison rate ~age	-0.009±0.004		12428	20
Divison rate ~age+age^2	**0.039±0.011**	**-0.002±0.0005**	**12408**	
Second generation late daughters				
Divison rate ~intercept only			5494	63.3
Divison rate ~age	0.009±0.004		5490.3	59.6
Divison rate ~age+age^2	**0.090±0.011**	**-0.004±0.0004**	**5430.7**	

710

Mortality rate

712 We fitted Gamma-Gompertz-Makeham related models to the survival data. GGM models were tested for

713 assumptions among parameters, for instance, whether shape and scale parameters are independent or

714 defined by a rate parameter. For late (Fig. 2D) and second generation late daughters (Fig. S3B), we

715 optimized the scaling of the mother to daughter state relationship (transmission factor) based on the age

716 at death state distribution of early daughters (or late daughters for second generation late daughters) (Fig.

717 S10). We assumed that accumulation of damage, which is the stage transition probabilities did not differ

718 among early, late and second generation late daughters. We also assumed that the effect of the stage was

719 not different for early, late or second-generation late daughters. These assumptions allowed us to use the

720 translated GGM estimates of the early daughters also for late and second generation late daughters.
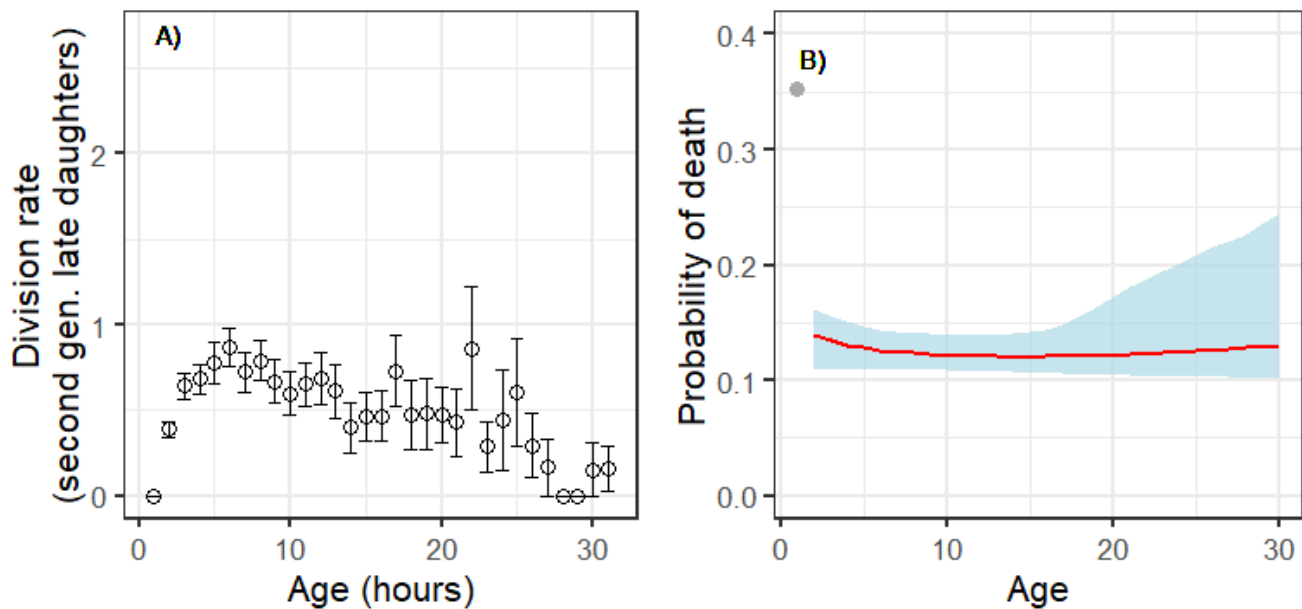
721

722 Fig. S3: Age-specific division rate (number of divisions per hour) (A) and age-specific hourly mortality

723 rate (B) of the 298 second generation late daughters. For (A) means ± standard errors are plotted, for (B)

724 fitted regression ± 95% Confidence Intervals are plotted. Associated model selection results are presented

725 in Table S2.

726

727 **Difference in mortality rates at old ages for early and late daughters**

728 The late age mortality plateau detected in early daughters (Fig. 2C) and the flat mortality hazard pattern

729 of the late daughters might indicate similar mortality rates at older ages (>19 hours). To test for this we

730 compared models that distinguished between early and late daughters but only included cells that

35

731   survived to an age of at least 20 hours. Late daughter cells have lower mortality rates ($q_x=0.1248\pm0.0191$

732   mean±Std.Err.) than early daughters at old ages ($q_x=0.2005\pm0.0168$ mean±Std.Err.) (Table S3) . This

733   result comprises 73 early daughters and 41 late daughters that lived longer than 19 hours.

734   Table S3: Model selection for age-specific mortality rates (q_x) of old (>19h) early daughters and old
735   (>19h) late daughters, based on binomial models.

Model	Estimate±Std. Error	Quadratic term	AIC	ΔAIC
Mortality ~intercept only			95.79	6.09
Mortality ~cell type	**-0.591±0.211**		**89.7**	

736

Cell elongation rates

738   We illustrate findings for cell elongation rates for early, late and second generation late daughters (Fig.

739   S2). When comparing linear models, the best fitted model for all three cell types was a model with a

740   linear and quadratic term, though the curvature was minimal for early daughters (Table S1). Early and

741   late daughters showing a decline in cell elongation rate with age, while second generation late daughters

742   patterns are less clear.

743

36
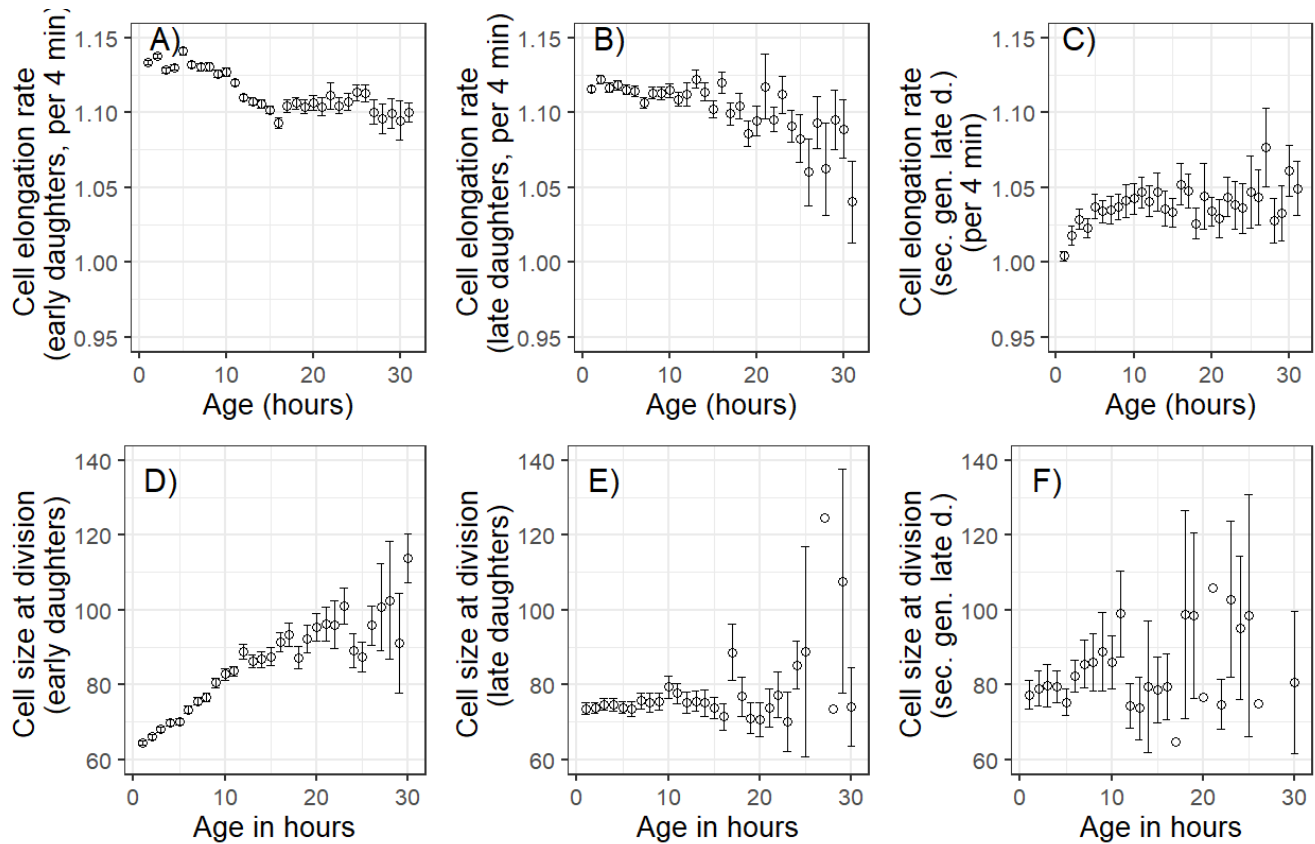
744

745   Fig. S2 Cell elongation and cell size:

746   A-C) Age-specific cell elongation rate (fractional elongation) and D-F) cell size at division (in pixels,

747   1pixel=0.064 µm) of the A&D) 516 early daughter cells, B&E) 516 late daughter cells, and C&F) 298

748   second generation late daughter cells. Hourly means ± standard errors are plotted. Associated model

749   comparisons are presented in Table S1).

750

751   Table S1: Model selection for age-specific cell elongation rates and cell size at division.

Model	Slope±Std. Error	Quadratic term	AIC	ΔAIC
Cell elongation rates				
Early daughters				
Elongation rate ~interc. only			-21415	407
Elongation rate ~age	-0.002±0.0001		-21820	2
Elongation rate ~age+age^2	**-0.002±0.0002**	**-0.00002±0.00001**	**-21822**	
Late daughters				

37

Model	Slope±Std. Error	Quadratic term	AIC	ΔAIC
Elongation rate ~interc. only			-10264	45
Elongation rate ~age	-0.00102±0.00016		-10304	5
Elongation rate ~age+age^2	**0.00013±0.00047**	**-0.000052±0.00002**	**-10309**	
Second generation late daughters				
Elongation rate ~interc. only			-4042.4	32.1
Elongation rate ~age	0.0014735±0.0002959		-4065.1	10.4
Elongation rate ~age+age^2	**0.00429±0.00088**	**-0.00012±0.000035**	**-4074.5**	
Cell size at division				
Model	**Slope±Std. Error**	**Quadratic term**	**AIC**	**ΔAIC**
Early daughters				
Size at division ~interc. only			53741	1378
Size at division ~age	1.72±0.04		52431	68
Size at division ~age+age^2	**2.797±0.135**	**-0.049±0.006**	**52362**	
Late daughters				
Size at division ~interc. only			28592	101
Size at division ~age	0.75±0.09		28525	34
Size at division ~age+age^2	2.204±0.259	-0.069±0.012	28491	
Second generation late daughters				
Size at division ~interc. only			8381.7	276.2
Size at division ~age	3.036±0.223		8215.9	110.4
Size at division ~age+age^2	**8.919±0.576**	**-0.293±0.027**	**8105.5**	

752

Size at division

753

754 We illustrate cell size at division for early, late, and second generation late daughters (Fig. S2). When

755 comparing linear models, the best fitted model for all three cell types was a model with a linear and

756 quadratic term, though the curvature was minimal for early and late daughters (Table S1). Early daughters

757 showed clear senescence in cell elongation rate, late daughters showed weaker senescence in cell

758 elongation rate, and patterns for second-generation late daughters are less clear.

759

38

Reverse time analyses: Hours before death

Chronological aging follows individuals from birth to death and time counted starts at birth. Various hypotheses about the evolution of life histories, aging and senescence, in particular, terminal investment strategies (Williams 1966, Clutton-Brock 1984, Charlesworth 1994), assume that individuals can sense that they are approaching death and that an optimal strategy for an individual might be to invest remaining resources into reproduction rather than maintenance when approaching immediate death. Such terminal investment has also been labeled as terminal illness, last year effect, or similar terms, and have been studied in a broad range of taxa, also using reverse time analyses (Coulson and Fairweather 2001). As Fig. 2 & Fig. 3 in the main text illustrates, age at death is highly variable, for that chronological senescence patterns and terminal investment strategies might provide very different insights. We investigated whether patterns in reproduction (division rate), cell elongation rate, or size at division differ significantly when time is counted backward (remaining lifespan), starting with death. We would expect that the last hour before death would show significant changes compared to the more spread out chronological senescence patterns (Fig. 2, Fig. S3 & S4). In general, there seems to be little evidence that terminal investment is happening to a larger degree, at least such strategies if existent, do not show larger effects compared to chronological aging and classical senescence (Fig. S5 & S6, Table S4 & S5).

Division rate for hours before death

When individual cells approach death, their division rates decrease (Fig. S5), and these senescence patterns are similar compared to the (chronological) senescence patterns (Fig. 2A, B) (Table S4 & Table S2).

39
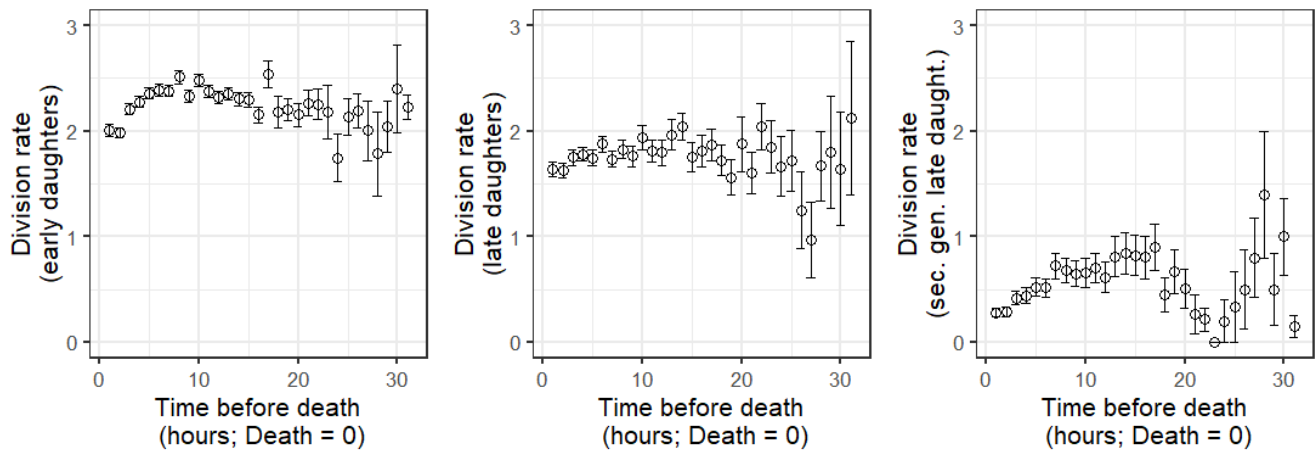
782

783   Fig. S5: Hourly division rate for hours before death [remaining life time] (death = time 0) for left panel

784   the 516 early daughters cells, mid panel the 516 late daughters, and right panel the 298 second generation

785   daughters. Means ± standard errors are plotted. Associated model selection is shown in Table S4.

786

787   Table S4: Model selection for division rate in reverse time (starting with age at death=0).

Model	Slope±Std. Error	Quadratic term	AIC	ΔAIC
Early daughters				
Division rate ~interc. only			19567	69
Division rate ~reverse time	0.006±0.002		19561	64
Division rate ~ reverse time + reverse time ^2	**0.062±0.0070**	**-0.002±0.0003**	**19497**	
Late daughters				
Division rate ~interc. only			12171	8
Division rate ~reverse time	0.006±0.003		12170	7
Division rate ~ reverse time + reverse time ^2	**0.036±0.017**	**-0.001±0.0004**	**12163**	
Second generation daughters				
Division rate ~interc. only			5474.5	47.8
Division rate ~reverse time	0.015±0.003		5456	29.3
Division rate ~ reverse time + reverse time ^2	**0.069±0.017**	**-0.002±0.0004**	**5426.7**	

788

789   **Cell elongation rate for hours before death**

790   The cell elongation rate does not drastically fall off when approaching death (no initial steep increase in

791   cell elongation rate close to the time of death) (Fig. S6, Table S5). The senescence pattern is, at least for

792   early and late daughters, less pronounced compared to that observed for chronological senescence (Fig.

793   S2). Second generation daughters seem to reduce cell growth rates before death more substantially, but

794   this reduction already starts a few hours before death and is not in line with terminal investment theories.
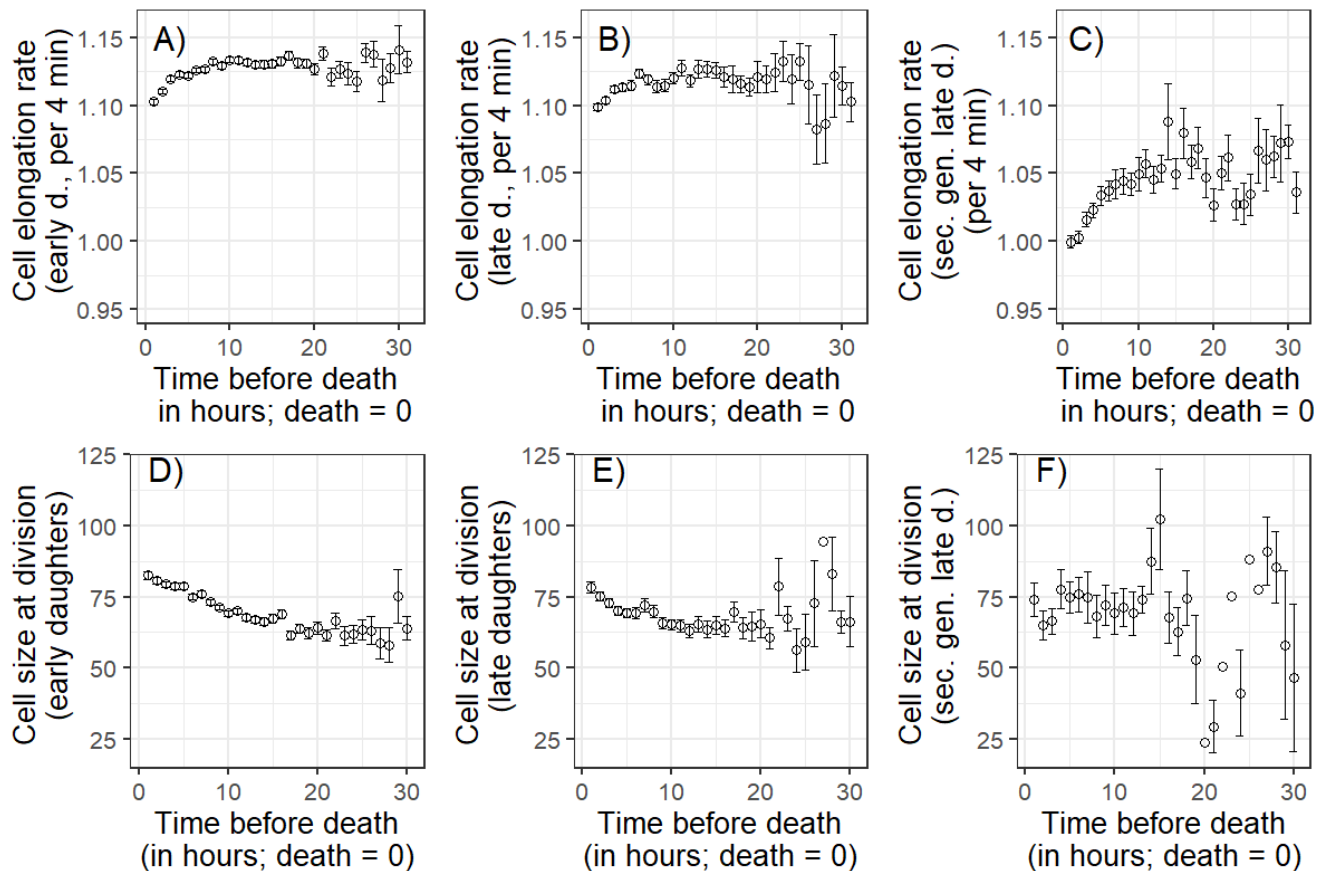
795

796   Fig. S6: (Fractional) Cell elongation rate and cell size at division (in pixels, 1pixel=0.064 µm) for hours

797   before death (death = time 0) for A & D) the 516 early daughters, B & E) the 516 late daughters, and C

798   & F) the 298 second generation late daughters. Means ± standard errors are plotted. Associated model

799   selection is shown in Table S5.

800

801 Table S5: Model selection for cell elongation and cell size at division rate in reverse time (starting with
802 age at death=0).

Model	Slope±Std. Error	Quadratic term	AIC	ΔAIC
Cell elongation (reverse time)				
Early daughters				
Elongation rate ~interc. only			-22138	250
Elongation rate ~reverse time	0.001±0.00009		-22288	100
Elongation rate ~ reverse time + reverse time ^2	**0.004±0.0003**	**-0.0001±0.00001**	**-22388**	
Late daughters				
Elongation rate ~interc. only			-10529	65
Elongation rate ~reverse time	0.001±0.0001		-10561	33
Elongation rate ~ reverse time + reverse time ^2	**0.003±0.0004**	**-0.0001±0.00002**	**-10594**	
Second generation late daughters				
Elongation rate ~interc. only			-4082.8	122.1
Elongation rate ~reverse time	0.003±0.0003		-4167.5	37.4
Elongation rate ~ reverse time + reverse time ^2	**0.008±0.0009**	**-0.0002±0.00003**	**-4204.9**	
Cell size at division (reverse time)				
Early daughters				
Size at division ~interc. only			53679	386
Size at division ~reverse time	-0.952±0.0486		53299	6
Size at division ~ reverse time + reverse time ^2	-1.337±0.145	0.018±0.006	53293	
Late daughters				
Size at division ~interc. only			28629	26
Size at division ~reverse time	-0.438±0.088		28606	3
Size at division ~ reverse time + reverse time ^2	**-0.990±0.258**	**0.026±0.011**	**28603**	
Second generation late daughters				
Size at division ~interc. only			8182.3	54.9

Size at division ~reverse time	1.254±0.236		8156.6	29.2
Size at division ~ reverse time + reverse time ^2	**4.531±0.627**	**-0.158±0.028**	**8127.4**	

803

Cell size at division for hours before death

805 Cell size at division increased with chronological age, but mainly for early daughters (Fig. S2). One

806 mechanism that might lead to such an increase in cell size at division is the formation of filamentous

807 cells: cells that do continue to elongate but stop dividing. Such filamentation is usually seen as a stress

808 response and increases mortality of the cell (Mattick et al. 2003, Wang et al. 2010). Previous studies

809 (conducted under different media and temperature than ours) have reported higher filamentation rates

810 with increasing age (Wang et al. 2010). Under our growth conditions, cells that entered a filamentation

811 stage rarely recovered from that stage and did not return to a regular dividing smaller cell, though they

812 not always stalled dividing. To test if such filamentous cells drive the chronological senescence pattern

813 in size at division, we investigated the cell size for the hours before death. For early and late daughters,

814 we detected an increase in cell size at division before death, but this increase is already initiated hours

815 before the actual death and not a final increase in size due to filamentation (Fig. S6, Table S5).

816

Random deterioration model

818 Our random deterioration model builds on a LeBras type cascading failure model(Le Bras 1976). In such

819 discrete state models, individuals increase from a current state *i* to a state *i+1* at a rate proportional to *i*,

820 and mortality increases proportionally to state *i*. We can think of such states as accumulating damage, or

821 model the reverse process, where an individual starts with some vitality and this vitality then decreases

822 with increasing state *i* (random deterioration) (Weitz and Fraser 2001). In this study, we assume

43

823   accumulating damage that stands symbolically for an unknown aging factor. These random deterioration

824   models are mathematically closely linked to demographic frailty models that do not assume a stochastic

825   stage progression among individuals, but rather heterogeneity of individual is defined by fixed frailty at

826   birth (Yashin et al. 1994). Such frailty, an age independent mortality that follows a gamma distribution

827   (Missov and Vaupel 2015), can be added to the classical models in demography, a Gompertz- model,

828   which describes an age-dependent exponential increase in mortality. These models can also be extended

829   by a Makeham term, an age-independent baseline mortality, which further improves model fit, at least

830   for humans and various other complex species.

831

832   We first estimated parameters of such a Gamma-Gompertz-Makeham (GGM) model, $Zae^{bx}+c$ fitted to

833   the survival data of the early daughters. Z is the random frailty variable that follows a gamma distribution

834   across individuals. The distribution has a mean 1 and variance of σ^2. This definition of a gamma

835   distribution with a mean of 1 implies that we have to set the scale parameter equal to the shape parameter

836   of the gamma distribution. The rate of aging, b, is the same for all individuals, x determines the age in

837   hours, a describes the baseline mortality of the Gompertz part of the model, and c describes the Makeham

838   term, the age independent mortality.

839

840   We then transformed these estimates of the GGM model to a random deterioration model according to

841   Yashin et al. (Yashin et al. 1994), making use of mathematical similarities between the GGM and random

842   deterioration models.

843   Let $t(i) = \lambda_0 + i\lambda$, $m(i) = \mu_0 + i\mu$ (for i greater than or equal to 0) denote the state transition rate and the

844   death rate, respectively.

845       $\mu_0 = a+c$, the death rate at birth i.e. state $i=0$,

44

846          $\lambda_0 = \frac{b}{\sigma^2} - a$, the transition rate from state i=0 to state i=1,

847          $\lambda = b - \sigma^2 a$, the change in the state transition rate between state i and $i+1$, for $i>0$

848          $\mu = \sigma^2 a$, the change in the death rate at state i, for $i>0$

849

850   Resulting estimates for early daughters were μ_0=0.056, $\lambda_0 = 0.178$, $\lambda = 0.598$, and $\mu = 0.00023$.

851   Using these estimates for early daughters, we estimated the probability of observing an individual at state

852   i at age x, $P(x,i)$,

853
$$P_i(x) = \begin{cases} P_0(0)e^{-(\lambda_0 + \mu_0)x} , & i = 0 \\ \frac{P_0(x)}{i!}\left[\frac{\lambda - \lambda e^{-(\lambda+\mu)x}}{\lambda + \mu}\right]\prod_{k=1}^{i}\left(\frac{\lambda_0}{\lambda} + (k-1)\right), & i > 0 \end{cases}$$

854   We then built a matrix of $P(x, i)$ for which we limited the age, x, between 0 and 31 and the states were

855   limited between 0 and 5000. The column sum of this matrix equals the survival probability at any given

856   age x to age $x+1$.

857   *Microsimulations of the random deterioration model*

858   In order to simulate the (damage) state at death distribution we used a microsimulation. As a step-by-

859   step calculation would take too long, we modelled the state at death distribution by drawing of a Poisson

860   distribution with a rate of $\frac{1}{\mu_0 + \hat{\imath}\mu}$, where $\hat{\imath} = i + \frac{1}{\mu_0 + i\mu}$. In doing so, we estimated the expected state at

861   death, rather than tracking individuals transitioning through damage states and their associated mortality

862   risk as a step-by-step calculation would do. A step-by-step simulation would take a long time because

863   individuals can easily end up in very high damage states (very long tailed distributions).

864

865   *Estimating parameters for the late daughters*

866   For the late daughters, we used the same state transition and survival parameters (μ_0=0.056, $\lambda_0 = 0.178$,

867    $\lambda = 0.598$, and $\mu = 0.00023$) that we estimated for the early daughters. We did so because early and

868   late daughter cells should biologically not be fundamentally different – aside of starting with different

869   damage levels at birth. They should accumulate damage at the same rate and should experience mortality

870   risk just based on their damage state. We assumed that the late daughters are born at the same stage, or a

871   scaled version of the same stage, in which the mothers died, therefore let

872    $$\lambda_{0,late} = nint(s(\lambda_{0,early} + i\lambda))$$

873    $$\mu_{0,late} = nint(s(\mu_{0,early} + i\mu))$$

874   Where subscript *late* and *early* denotes late and early daughter estimates and $s \in (0,1)$ and $nint(.)$ is

875   the nearest integer function. So based on the estimated damage state distribution of the mothers at death

876   (early daughters), we also knew the damage state distribution at birth of the daughters (late daughters)

877   [see below for optimally scaling this distribution]. Using the state transition probabilities of the early

878   daughters and the probabilities of death, we estimated the survival of the late daughters. We also

879   estimated the survival functions of cells that did not change their damage state with age. Each grey line

880   in main text Fig. 3, describes such a fixed damage class survival function.

881   In order to determine the transmission fraction of accumulated damage between mothers (early

882   daughters) and daughters (late daughters), we optimized the scaling of the mother state at death

883   distribution (fraction of mother-daughter transmission) to the daughter age at birth distribution. The

884   optimization was based on observed survival of the late daughters, by minimizing the squared deviations

885   from the observed survival function. This optimal scaling factor was estimated at 7%.

886   Similar to the late daughters, we simulated the damage state distribution at birth, the damage state

887   distribution at death, and calculated the matrix $P(x,i)$ for the second generation late daughters.

46
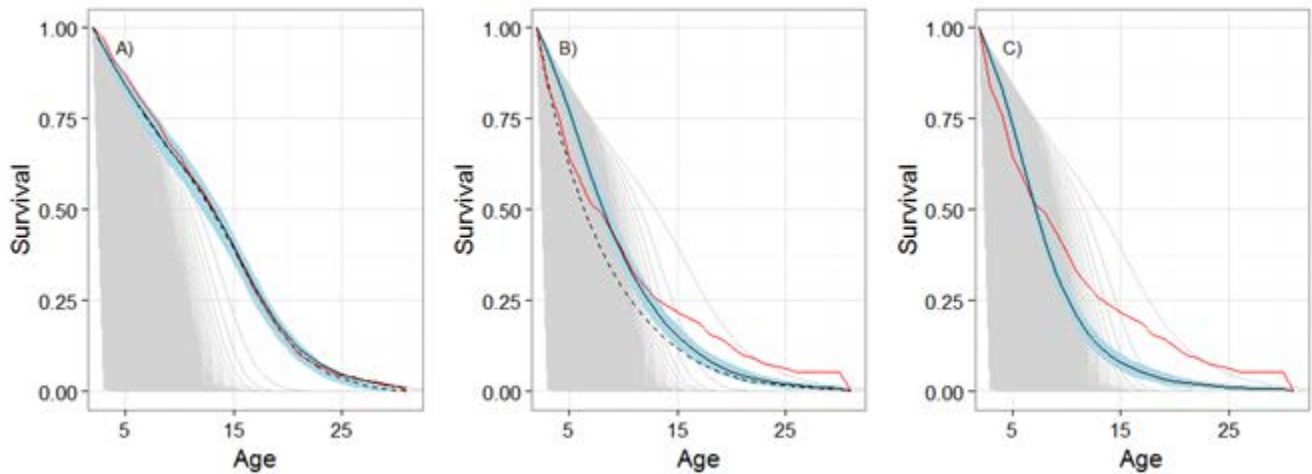
Fig. S9: Observed population level survival curve (red line), GGM simulated survival curve with symmetric damage transmission (hatched black line) as well as GGM simulated survival curve with asymmetric damage transmission of 7% (solid black line ± 95% CI in blue) for early (A), late (B) and second generation late daughters (C). Graphs A & B are identical to Fig. 1C & D. Thin grey lines in depict expected survival curve of cells with different fixed damage state. That is, for instance, the outermost thin grey line in B depicts the survivorship curve of a hypothetical cohort that starts without damage and never accumulates any damage. The most left survival curve illustrates the low survival of cells that were born with maximum damage level of 5000.
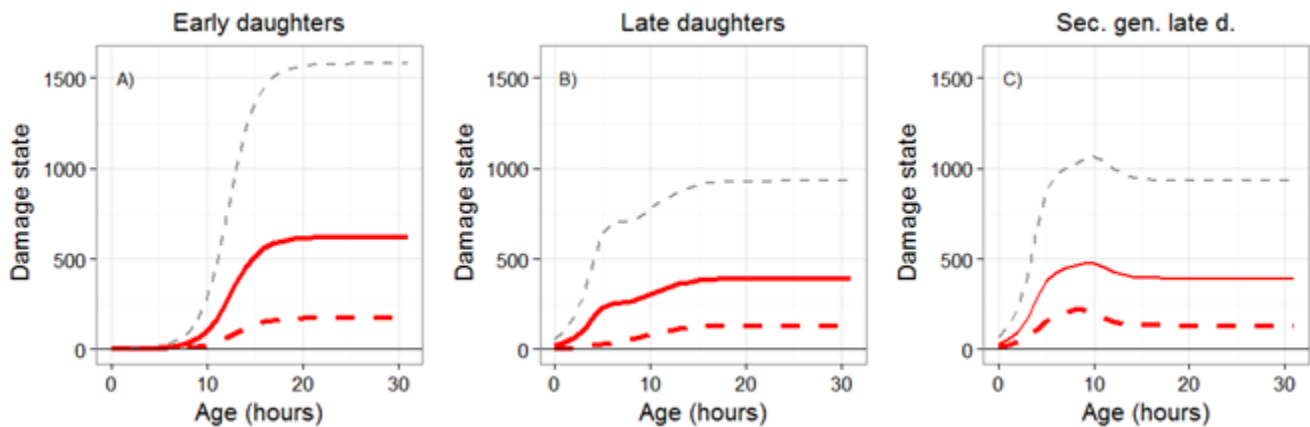
47
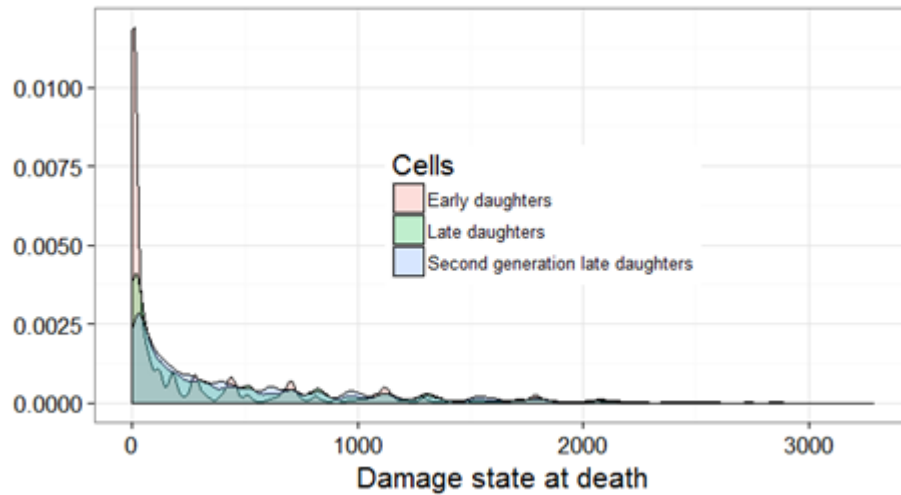
898

899 Fig. S10: Density distribution of damage state at death of early daughters, late daughters, and second

900 generation late daughters. Most cells die with little accumulated damage. Note, the not so smooth tails

901 of the distributions are a result of drawing from a Poisson distribution in our simulations.
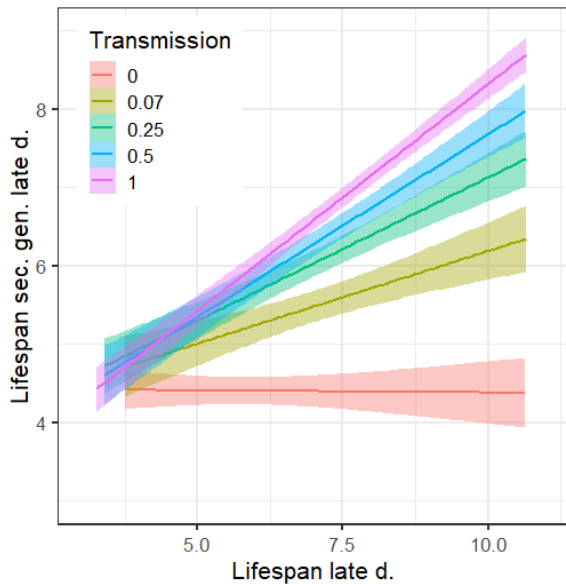
902

903

904 Fig. S11: GGM model results: mean (red solid line, + SD grey hatched lines) and median (red hatched

905 line) damage state with increasing age for early daughter cells (A), and late daughter cells (B) and second

906 generation late daughter cells (C). Panel A & B are identical to Panel Fig. 1A, B.

907

48

908

909 Fig. S12: Lifespan (square root transformed) of simulated 516 late daughter cells (mothers) versus the

910 lifespan of their simulated last daughter cell (second generation late daughter cells) with different levels

911 of mother to daughter damage transmission. Scenarios include the optimized fixed transmission level at

912 0.07 (forest green), a scenario for perfect rejuvenation, i.e. 0 transmission (red), 0.25 transmission

913 (green), 0.5 transmission, i.e. symmetric (equal) transmission between mother and daughter (blue), and

914 transmission of all accumulated damage to the daughter (1) (pink).CI are shown for each correlation in

915 lifespan between mothers and daughters as shaded areas.

916

917 **References**

918 Ackermann, M. 2015. A functional perspective on phenotypic heterogeneity in microorganisms. - Nat.

919   Rev. Microbiol. 13: 497–508.

920 Ackermann, M. et al. 2003. Senescence in a bacterium with asymmetric division. - Science 300: 1920.

921 Ackermann, M. et al. 2007. On the evolutionary origin of aging. - Aging Cell 6: 235–44.

922   Aoki, S. K. et al. 2005. Contact-Dependent Inhibition of Growth in Escherichia coli. - Science (80-.).

923   in press.

924   Balázsi, G. et al. 2011. Cellular decision making and biological noise: from microbes to mammals. -

925   Cell 144: 910–925.

926   Blattner, F. R. 1997. The Complete Genome Sequence of Escherichia coli K-12. - Science (80-.). 277:

927   1453–1462.

928   Brillinger, D. R. 1986. A Biometrics Invited Paper with Discussion: The Natural Variability of Vital

929   Rates and Associated Statistics. - Biometrics 42: 693.

930   Burnham, K. and Anderson, D. R. 1998. Model selection and multimodel inference : a practical

931   information-theoretic approach. - Springer.

932   Caswell, H. 2001. Matrix population models: construction, analysis, and interpretation. - Sinauer

933   Associates.

934   Charlesworth, B. 1994. Evolution in age-structured populations. - Cambridge University Press.

935   Clutton-Brock, T. 1984. Reproductive effort and terminal investment in iteroparous animals. - Am.

936   Nat. 123: 212–229.

937   Coquel, A.-S. et al. 2013. Localization of protein aggregation in Escherichia coli is governed by

938   diffusion and nucleoid macromolecular crowding effect. - PLoS Comput. Biol. 9: e1003038.

939   Coulson, J. C. and Fairweather, J. A. 2001. Reduced reproductive performance prior to death in the

940   Black-legged Kittiwake: senescence or terminal illness? - J. Avian Biol. 32: 146–152.

941   Davidson, C. J. and Surette, M. G. 2008. Individuality in Bacteria. - Annu. Rev. Genet. 42: 253–268.

942   Denoth Lippuner, A. et al. 2014. Budding yeast as a model organism to study the effects of age. -

943   FEMS Microbiol. Rev. 38: 300–25.

944   Elowitz, M. B. et al. 2002. Stochastic gene expression in a single cell. - Science (80-.). 297: 1183–

945   1186.

946   Evans, S. N. and Steinsaltz, D. 2007. Damage segregation at fissioning may increase growth rates: a

947   superprocess model. - Theor. Popul. Biol. 71: 473–90.

948   Finch, C. and Kirkwood, T. B. 2000. Chance, Development, and Aging. - Oxford University Press.

949   Gangan, M. S. and Athale, C. A. 2017. Threshold effect of growth rate on population variability of

950   Escherichia coli cell lengths. - R. Soc. open Sci. 4: 160417.

951   Gasset-Rosa, F. et al. 2014. Direct assessment in bacteria of prionoid propagation and phenotype

952   selection by Hsp70 chaperone. - Mol. Microbiol. 91: 1070–87.

953   Hamilton, W. D. 1966. The moulding of senescence by natural selection. - J. Theor. Biol. 12: 12–45.

954   Jagers, P. 1978. Balanced exponential growth: what does it mean and when is it there? - In:

955   Biomathematics and cell kinetics. Elsevier, pp. 21–29.

956   Johnson, L. R. and Mangel, M. 2006. Life histories and the evolution of aging in bacteria and other

957   single-celled organisms. - Mech. Ageing Dev. 127: 786–93.

958   Jones, O. R. et al. 2014. Diversity of ageing across the tree of life. - Nature 505: 169–73.

959   Jouvet, L. et al. 2017. Demographic variability and heterogeneity among individuals within and among

960   clonal bacteria strains. - Oikos in press.

961   Kærn, M. et al. 2005. Stochasticity in gene expression: from theories to phenotypes. - Nat. Rev. Genet.

962   6: 451–464.

963   Kennedy, B. K. 1994. Daughter cells of Saccharomyces cerevisiae from old mothers display a reduced

964   life span. - J. Cell Biol. 127: 1985–1993.

965   Kirkwood, T. B. L. 2005. Understanding the odd science of aging. - Cell 120: 437–47.

966   Kirkwood, T. B. L. et al. 2005. What accounts for the wide variation in life span of genetically identical

967   organisms reared in a constant environment? - Mech. Ageing Dev. 126: 439–443.

968   Klein, J. P. and Moeschberger, M. L. 2003. Survival analysis : techniques for censored and truncated

969   data. - Springer.

970   Le Bras, H. 1976. Lois de mortalité et age limite. - Population (Paris). 33: 655–691.

971   Lindner, A. B. and Demarez, A. 2009. Protein aggregation as a paradigm of aging. - Biochim. Biophys.

972   Acta 1790: 980–96.

973   Lindner, A. B. et al. 2008. Asymmetric segregation of protein aggregates is associated with cellular

974   aging and rejuvenation. - Proc. Natl. Acad. Sci. U. S. A. 105: 3076–81.

975   López-Otín, C. et al. 2013. The hallmarks of aging. - Cell 153: 1194–217.

976   Mattick, K. et al. 2003. Morphological changes to Escherichia coli O157:H7, commensal E. coli and

977   Salmonella spp in response to marginal growth conditions, with special reference to mildly

978   stressing temperatures. - Sci. Prog. 86: 103–113.

979   Medawar, P. B. 1952. An unsolved problem of biology. - In: Uniqueness of the Individual. H. K.

980   Lewis, in press.

981   Minois, N. et al. 2005. Advances in measuring lifespan in the yeast Saccharomyces cerevisiae. - Proc.

982   Natl. Acad. Sci. U. S. A. 102: 402–6.

983   Missov, T. I. and Vaupel, J. W. 2015. Mortality Implications of Mortality Plateaus. - SIAM Rev. 57:

984   61–70.

985   Norman, T. M. et al. 2013. Memory and modularity in cell-fate decision making. - Nature 503: 481–

986   486.

987   Norman, T. M. et al. 2015. Stochastic Switching of Cell Fate in Microbes. - Annu. Rev. Microbiol. 69:

988   381–403.

989   R Core Team, R. A. language and environment for statistical computing. 2016. R: A language and

990   environment for statistical computing. (RDC Team, Ed.). - R Found. Stat. Comput. 1: 409.

991 Scherbov, S. and Ediev, D. 2011. Significance of life table estimates for small populations: Simulation-

992   based study of estimation errors. - Demogr. Res. 24: 527–550.

993 Steiner, U. K. and Tuljapurkar, S. 2012. Neutral theory for life histories and individual variability in

994   fitness components. - Proc. Natl. Acad. Sci. U. S. A. 109: 4684–9.

995 Steinsaltz, D. and Evans, S. N. 2004. Markov mortality models: implications of quasistationarity and

996   varying initial distributions. - Theor. Popul. Biol. 65: 319–37.

997 Stewart, E. J. et al. 2005. Aging and death in an organism that reproduces by morphologically

998   symmetric division. - PLoS Biol. 3: e45.

999 Stroustrup, N. et al. 2016. The temporal scaling of Caenorhabditis elegans ageing. - Nature 530: 103–

1000   107.

1001 Tyedmers, J. et al. 2010. Cellular strategies for controlling protein aggregation. - Nat. Rev. Mol. cell

1002   Biol. 11: 777–788.

1003 Vaupel, J. W. and Yashin, A. I. 1985. Heterogeneity's Ruses: Some Surprising Effects of Selection on

1004   Population Dynamics. - Am. Stat. 39: 176.

1005 Vaupel, J. W. et al. 1998. Biodemographic Trajectories of Longevity. - Science (80-.). 280: 855–860.

1006 Vaupel, J. W. et al. 2004. The case for negative senescence. - Theor. Popul. Biol. 65: 339–351.

1007 Vera, M. et al. 2016. Single-Cell and Single-Molecule Analysis of Gene Expression Regulation. -

1008   Annu. Rev. Genet. 50: 267–291.

1009 Wachter, K. W. 1999. Evolutionary demographic models for mortality plateaus. - Proc. Natl. Acad. Sci.

1010   96: 10544–10547.

1011 Wachter, K. W. et al. 2014. Evolutionary shaping of demographic schedules. - Proc. Natl. Acad. Sci. U.

1012   S. A. 111 Suppl: 10846–53.

1013 Wang, P. et al. 2010. Robust growth of Escherichia coli. - Curr. Biol. 20: 1099–103.

1014   Weitz, J. and Fraser, H. 2001. Explaining mortality rate plateaus. - Proc. Natl. Acad. Sci. U. S. A. 98:

1015   15383–15386.

1016   Williams, G. C. 1957. Pleiotropy, Natural Selection, and the Evolution of Senescence. - Evolution (N.

1017   Y). 11: 398.

1018   Williams, G. C. 1966. Adaptation and natural selection : a critique of some current evolutionary

1019   thought. - Princeton Univeristy Press.

1020   Wolf, M. et al. 2007. Life-history trade-offs favour the evolution of animal personalities. - Nature 447:

1021   581–584.

1022   Yashin, A. I. et al. 1994. A duality in aging: the equivalence of mortality models based on radically

1023   different concepts. - Mech. Ageing Dev. 74: 1–14.

1024